Theses of

Master Thesis

Stochastic Analysis of Interfacial Effects on the Polymeric Nanocomposites

Submitted by
Ashkan Almasi
Matriculation number: 112549

Reg.-Nr.: NHRE/2014/13

BAUHAUS-UNIVERSITÄT WEIMAR
Faculty of Civil Engineering
Institute of Structural Mechanics

DECLARATION

Hereby, I declare that I worked on this Master Thesis independently and using only the specified sources and programs which are referred.

Ashkan Almasi

DEDICATION

This Master thesis is dedicated to my bests in my life: My parents, Farjollah Almasi and Parvin Siahat Shayesteh

ACKNOWLEDGEMENTS

The research reported in this dissertation has been carried out in the Institute of Structural Mechanics, Faculty of Civil Engineering of Bauhaus-Universität Weimar, Germany. I would like to express my deepest gratitude to my thesis supervisor, Prof. Dr.-Ing. Timon Rabczuk, for having accepted me as his Master student. I would also like to express my sincere gratitude to my co-supervisor Dr. Mohammad Silani for the continuous support of my Master study and research, for his patience, motivation, enthusiasm, and immense knowledge. Moreover, I would like to specially thank Dr. Hossein Talebi for his constructive comments and various advices and additionally I am grateful to Dr. Behroz Arash for many discussions and support.

Last but not least, I would like to express my biggest gratitude to my family specially my mother for everything.

Abstract

The polymeric clay nanocomposites are a new class of materials of which recently have become the centre of attention due to their superior mechanical and physical properties. Several studies have been performed on the mechanical characterisation of these nanocomposites; however most of those studies have neglected the effect of the interfacial region between the clays and the matrix despite of its significant influence on the mechanical performance of the nanocomposites.

There are different analytical methods to calculate the overall elastic material properties of the composites. In this study we use the Mori-Tanaka method to determine the overall stiffness of the composites for simple inclusion geometries of cylinder and sphere. Furthermore, the effect of interphase layer on the overall properties of composites is calculated. Here, we intend to get bounds for the effective mechanical properties to compare with the analytical results. Hence, we use linear displacement boundary conditions (LD) and uniform traction boundary conditions (UT) accordingly. Finally, the analytical results are compared with numerical results and they are in a good agreement.

The next focus of this dissertation is a computational approach with a hierarchical multiscale method on the mesoscopic level. In other words, in this study we use the stochastic analysis and computational homogenization method to analyse the effect of thickness and stiffness of the interfacial region on the overall elastic properties of the clay/epoxy nanocomposites. The results show that the increase in interphase thickness, reduces the stiffness of the clay/epoxy naocomposites and this decrease becomes significant in higher clay contents. The results of the sensitivity analysis prove that the stiffness of the interphase layer has more significant effect on the final stiffness of nanocomposites. We also validate the results with the available experimental results from the literature which show good agreement.

TABLE OF CONTENTS

LIST OF TABLES

LIST OF FIGURES

Chapter 1

Introduction

1.1 Introduction

Polymeric clay nanocomposites are a new class of materials which have been the subject of extensive researches recently owing to their outstanding mechanical properties. These materials have great multifunctional thermo-mechanical properties such as low permeability and flame retardancy, which are the results of using high aspect ratio clays inside the polymeric matrix. The high aspect ratios make a huge amount of interfacial connections between clays and matrix [1, 2, 3]. The interface is defined as the first few molecular layers close to the solid surface that are responsible for the adhesion between two materials. Far from the solid surface, the properties of polymer is same as the bulk polymer, while the properties of the polymer near to the interface differ from that of the bulk polymer due to the influence of the interface adhesion. This region is called interphase, see Fig. 1.1. Interfaces and interphases play a significant role in the global properties of the nanocomposites [4, 5, 6, 7]. The thickness of the interphase region is in the order of nanometers. Meanwhile this very small thickness makes the experimental investigations limited, expensive and in some cases impractical to make an estimate of mechanical properties.

Some analytical models were proposed in the literature to determine the mechanical properties of the overall composite in the presence of interphase layer for simple geometries. Odegard et al. [8] used the Mori-Tanaka method [9, 10] to determine the elastic properties of three-phase composites i.e. matrix, inclusion and the interphase zone. They

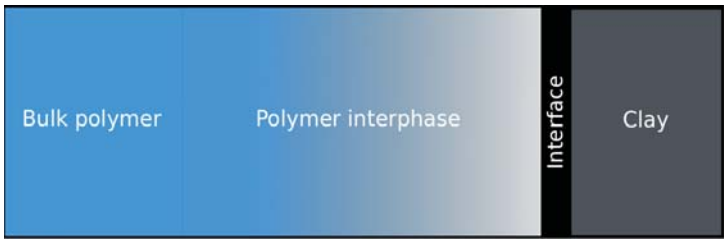

Figure 1.1: The schematic illustration of the microstructure of the clay/epoxy nanocomposite with the interface and interphase layers

also presented the "effective interface model" for an spherical inclusion. Sevostianov and Kachanov [11] presented the concept of equivalent homogeneous inclusion method. This method considers the interphase layer and particle as one-phase and matrix as another. However, the lack of exact deterministic values for the interfacial behaviours of the polymeric nanocomposites limits the use of the analytical methods for deterministic models.

There are comprehensive studies by Molecular Dynamics (MD) to determine the mechanical characterization of nanocomposites [12, 13, 14, 15]. Chen et al. [16] investigated the mechanical properties of the interfaces in clay/epoxy nanocomposites based on the concept of binding energy in the MD simulations. Odegard et al. [8] used Monto Carlo (MC) and MD simulations to predict the elastic properties of silica nanoparticle/polyimide composites. Tsai et al. also [17] presented a multiscale simulation approach to characterize the elastic properties of carbon nanotubes (CNTs) reinforced polyimide nanocomposites. They also introduced an effective interphase between the CNTs and polyimid polymer to evaluate the degree of non-bonded interaction through MD simulations. Using MD simulations, Arash et al. [18] proposed a method to evaluate elastic properties of the interfacial region that was developed by examining the fracture behaviour of CNTs reinforced polymer composites.

Although MD simulations can provide some insight to the interphase zone in the nanocomposites, the limitation of RVE size in MD simulations has encouraged the researchers to use finite element method in the meso-scale [19, 20, 21, 22, 23]. Vu-Bac et al. [24] proposed a stochastic framework based on sensitivity analysis (SA) methods to quantify the key input parameters influencing the Young's modulus of polymer (epoxy) clay nanocomposites (PCNs). Silani et al. [25] presented a numerical investigation of the mechanical properties of exfoliated clay/epoxy nanocomposites. All of these studies have neglected the effect of interphase region which plays a very important role in the

mechanical properties. Therefore, in this study we investigate the effect of the interphase layer on the elastic properties of PCNS. We used a combination of the stochastic analysis and micromechanical method using the finite element method. We have considered an equivalent model to capture both interface and interphase regions in a finite element model. The numerical results show that in the elastic region, the interfacial region is significant when the thickness of the equivalent model is thick enough. We also verify our numerical results with that of the experimental observations that show a very good agreement.

The master thesis is organized as follows. Chapter 2 contains an introduction to nanocomposites and their application areas. Chapter 3 presents the results of different analytical methods as well as finite element method to predict the overall stiffness of nanocomposites for simple inclusion geometries. Chapter 4 describes the methodology to obtain mechanical properties of the clay/epoxy nanocomposites using the stochastic analysis. This chapter also includes the results and discussion. Finally in Chapter 5 we conclude the thesis.

Chapter 2

Nanocomposite materials

2.1 Nanocomposites

Polymeric materials are the class of material that are reinforced by stiff filler to promote mechanical properties. There are some main factors which are affected on the efficiency of reinforcement such as the filler aspect ratio, the filler mechanical properties and the adhesion between the matrix and the filler [26].

Since over the last decades the polymer/clay nanocomposites are widely used due to their special attributes: light-weight, low-cost, ease production and often ductile nature, considerable investigation was performed on physical properties of various polymer/clay nanocomposites [3].

In general view, polymeric nanocomposites were considered as a kind of materialt to improve thermal/mechanical properties over the matrix polymer. Moreover the productivity of reinforcement depends on different factors including the morphology of nanocomposites (exfoliated particle structure), the orientation of the clay platelets, the crystallinity (amorphous or semi-crystalline), the thermophysical properties (thermoplastic, epoxy or elastomer) of the matrix and the adhesion between the matrix and the nanoclay [26].

Polymer nanocomposites are composed of dispersing a filler material as a flat plates which are distributed into polymer matrix. Although, there are different type of fillers, the most common is nanoclay material which is called montmorillonite (a layered semec-

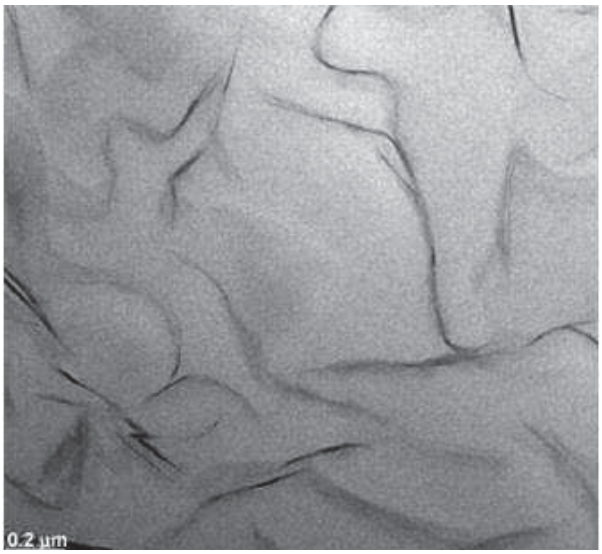

Figure 2.1: TEM micrographs of a clay/expoxy nanocompsoite [28].

tite clay). In nature, clays are hydrophilic while polymers are hydrophobic. In order to produce nanocomposites with nanofillers, there three common methods: melt compounding, in-situ polymerization and the solvent method [27].

Nanocomposite materials like other heterogeneous materials consist of clearly distinguishable constituents which show different mechanical and physical properties. Nanoscale interactions between components in nanocomposites result in an interesting and sometimes incredible properties which is not accessible in conventional materials. The exceptional specific strength (strength-to-weight ratio), enhancement in thermal and mechanical properties and multifunctional behaviours in nanocomposites have increased the global interest in this class of materials. Fig.2.1 shows TEM micrographs of polymeric clay nanocomposites that are a new class of materials which have been the subject of extensive researches during the last years. These materials have great multifunctional thermo-mechanical properties such as low permeability and flame retardancy which are the results of using high aspect ratio clays inside polymeric matrix. These high aspect ratio clays make a huge amount of interfacial connections between clays and matrix.

The performances of polymeric nanocomposites are governed by several factors. One is the large difference in material properties of the clays and the polymer matrix. Another important factor, of even greater significance given the large surface area to volume ratio, is the interface between the clays and the polymer matrix which affects the load transfer and thereby directly impacting the stiffness of the nanocomposite, strength, and

the effective thermal and electrical conductivity. Given the challenges associated with directly probing materials at the nanoscale, it is difficulty to conduct experiments to directly explore the interface in nanocomposites. Hence, there is increasing interests and reliance on computational materials science techniques to study the interface between the clays and the polymer matrix using analytical or numerical techniques such as atomistic simulation and the continuum models.

2.2 Classification of nanocomposites

Based on engineering application the nanocomposites are classified into two groups: non-polymer based nanocomposites and polymer based nanocomposites.

2.2.1 Non-polymer based nanocomposites

Non-polymer based nanocomposites can be classified into three major types of nanocomposites as below,

Metal/Metal Nanocomposite

Bimetallic nanomaterials is composed of magnetic metals and noble metals. Because of special properties of biometallic nanomaterials like, their magnetic, catalystic and optical properties, they have provided much interest application in the field of magnetic sensor, catalysts, optical detection and biomedical application.

Metal/Ceramic Nanocomposites

In the case of Metal/Ceramic Nanocomposites the electric, magnetic, chemical, optical and mechanical properties are combined for both phases. By reducing the size of components to the nanoscale, above mentioned properties was improved and leads to new application.

Ceramic/Ceramic Nanocomposites

Ceramic Nanocomposites could solve the problem of fracture failures in artificial joint implants, this will extend patient mobility and discard the high cost of surgery.

2.2.2 polymer based nanocomposites

Polymer nanocomposites are the kinds of composites with internal structure (a polymer matrix and filler) with at least one dimension less than 100 nm. The inclusions can be clay, nanotubes, platelets and nanoparticles.

Polymer/Ceramic nanocomposite

Nanocomposites composed of single ceramic layers (1nm thick) homogeneously dispersed in a continuous matrix. The host ceramic layer tend to orient themselves parallel with respect to each other due to dipole-dipole interaction.

Inorganic/Organic polymer nanocomposites

Metal polymer nanocomposites attracted considerable attention due to the unique properties of metal clusters which are dispersed in polymer matrix. For metal cluster the typical size is approximately 1-10 nm. The size and grains depends on mobility of the metal atoms on the polymer surface.

Inorganic/Organic hybrid nanocomposite

Inorganic/Organic hybrid nanocomposite are not simply physical mixtures, they can be widely determined components intimately mixed.

Polymer/ Layered silicate Nanocomposites

Polymer/Layered silicate (PLS) nanocomposites materials are attracting great interest in polymer science research. In recent years the PLS nanocomposites have attracted

significant interest both in industry and academia, because they often exhibits noticeable progressions in materials when compare with virgin polymer and typical macro and macro composites.

Polymer/polymer Nanocomposites

Polymers are more than ever under pressure to be chip and offered property profiles.

Biocomposites

Metals and metal alloys are used in orthopaedics, dentistry and other load bearing applications. Because of chemically inert nature or high bioactivity properties, ceramics are widely used. On the other hand polymers are used in many other non-structural application such as soft tissue replacements.

2.3 Nanocomposite properties

There are numerous advantages of nanocomposites and possibilities application for packaging industry. Due to the following properties, the nanocomposites are utilized in industry [27],
-Gas, oxygen, water,etc. barrier properties
-high mechanical strength
-Thermal stability
-Chemical stability
-Recyclability
-Heat resistance
-Good optical clarity (since particles are nano-size).

Fig.2.2 shows some examples of hybrid materials based on nanoparticles (NPs) and polymer nanocomposites (PNCs). Commercial developments of PNCs involve mainly two types of nano-objects: oxide-based particles (silica-based particles most of the time) and clays. This figure also illustrate; (a) interior footwell heater vent (Audi and Volkswagen models), (b) seat back (Honda Acura TL), (c) hull and deck of personal watercraft

Figure 2.2: Some commercial products based on polymer nanocomposites (PNCs) [29].

(Yamaha Motor Corporations WaveRunners), (d) trim, centre bridge, sail panel and box rail protector (GM Hummer H2 SUT), (e) centre console (Chevrolet HHR), (f) Michelin-Wocos antivibration systems (hybrid silica nanoparticles) and (g) Pirellis tyres based on cap (hybrid silica nanoparticles-based PNCs) and base (nanoclay-based PNCs) technology (h) Nanomer, (i) Nanolok and (j) Durethan PNCs [29].

2.3.1 Gas barrier properties

Fig.2.3 shows that clays are believed to increase the barrier properties by creating a maze or tortuous path that retards the progress of the gas molecules through the matrix resin. By comparing nanocomposites made with layered silicates of various aspect ratios, the permeability was seen to decrease with increasing aspect ratio [30].

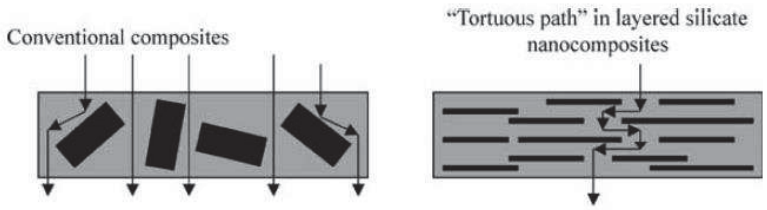

Figure 2.3: Formation of tortuous path in polymer/layered silicate (PLS) nanocomposites [30].

2.3.2 Fire retardant properties

Fire-relevant properties such as the heat release rate (HRR), heat peak HRR, smoke production, and CO2 yield, are vital to the evaluation of the fire safety of materials. The amount of smoke evolved and specific extinction area also decrease with the formation of the nanocomposites. There is some variability in the smoke production. Although it is observed that the formation of the nanocomposites reduces smoke production, the presence of additional clay does not continue this smoke reduction [30].

2.3.3 Thermal stability

The thermal stability of polymeric materials is usually studied by thermogravimetric analysis (TGA). The weight loss due to the formation of volatile products after degradation at high temperature is monitored as a function of temperature. When the heating occurs under an inert gas flow, a non-oxidative degradation occurs, while the use of air or oxygen allows oxidative degradation of the samples. Generally, the incorporation of clay into the polymer matrix was found to enhance thermal stability by acting as a superior insulator and mass transport barrier to the volatile products generated during decomposition [30].

2.3.4 Ionic conductivity

Solvent-free electrolytes are of much interest because of their charge-transport mechanism and their possible applications in electrochemical devices [30].

2.3.5 Other properties

PLS nanocomposites also show improvement in most general polymeric properties. For example, in addition to the decreased permeability of liquids and gases, nanocomposites also show significant improvement in solvent uptake. Scratch resistance is another property that is strongly enhanced by the incorporation of layered silicates [31].

Chapter 3

Homogenization

3.1 Fundamental Microstructural Definitions

Heterogeneous materials are composed of multiple phases. Fig.3.1a shows these phases which may be very complex. In Fig.3.1a a dipicted box demonstrate a particular portion of microstructure for investigation that is refered to as a sample and denoted by S. A two phases heterogeneous material is considered to introduce the main concepts and notation. Fig.3.1b shows a sample which is depicted from such material. A sample consist of two phases, the matrix phase is composed of material $M^{(1)}$ and occupies a portion of $\nu_0^{(1)}$ and the inclusion phase of material $M^{(2)}$ and occupies a portion of $\nu_0^{(2)}$ of ν, where $\nu_0^{(1)} \cup \nu_0^{(2)} = \nu_0$ and $\nu_0^{(1)} \cap \nu_0^{(2)} = 0$. There are two fundamental microstructure definition:

Definition 1. The Volume fraction of phase I and II are,

$$\begin{aligned} \nu_1 &= \frac{\left|\nu_0^{(1)}\right|}{|\nu_0|} \\ \nu_2 &= \frac{\left|\nu_0^{(2)}\right|}{|\nu_0|} \end{aligned} \tag{3.1}$$

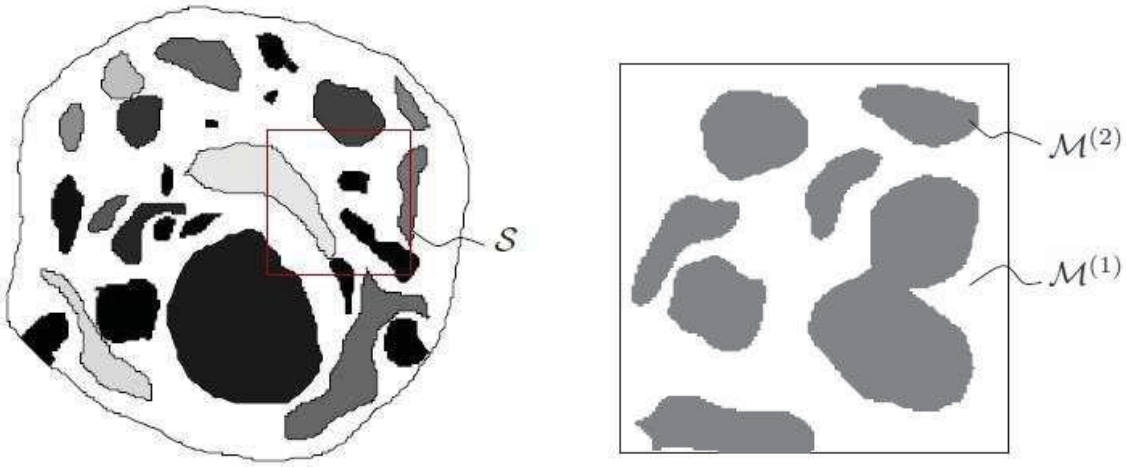

(a) (b)

Figure 3.1: A portion of a microstructure: (a) multiple phases, (b) two phases [32].

By definition, $\nu_1 + \nu_2 = 1$ and $\nu_0^{(1)} \neq \nu_1$.

Definition 2. The Volume average of quantity Q over a region Ψ is

$$\langle Q \rangle_\Psi = \frac{1}{|\Psi|} \int_\Psi Q \, d\Psi \tag{3.2}$$

3.2 Classification of Microstructures

3.2.1 Randomness and Periodicity

One method to classify the microstructure is to determine weather it displays randomness or periodicity. In the case of periodicity, the position and the orientation of particles are the same, which is shown in Fig.3.2a with 8^2 particles. Fig.3.2b demonstrates the randomness, the position and the orientation of particles are random with the same number of particles (8^2). Furthermore, they do not overlap and intersection and they have same size. Fig.3.2c shows that the particles lie over the boundaries and overlap and intersection are allowed and the size of the particles may vary. Monodisperse presented the particle system where the size and shape of the particles are the same, otherwise they are classified as polydisperse.

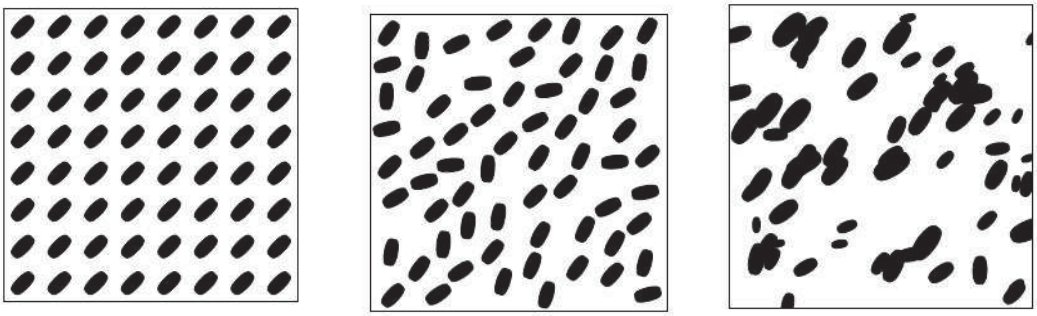

(a) (b) (c)

Figure 3.2: Geometrical classification of the microstructure: (a) periodic, (b) monodisperse random, (c) polydisperse random, with flexibility in the positions of the particles [32].

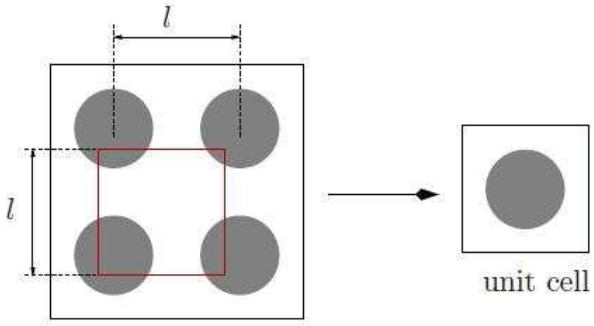

Figure 3.3: The unit cell from a periodic microstructure [32].

Fig.3.3 shows the unit cell which is related to the periodicity that is the simplest repeating substructure. As depicted in figure, the choice of unite cell is not unique. It should be mentioned that the size of unit cell must match with the length of periodicity (l) or be an integer multiple l. For the particulate composite, the simplest unit cell is one that encloses a particle.

3.2.2 Statistical Homogeneity

Another classification method is to differentiate features of the microstructures. One feature is the statistically homogeneous of the distribution of the inclusions which is shown in Fig.3.4a. Since the geometry of the microstructures does not change from point to point, the microstructure display the statistical homogeneity. Otherwise, the geometry of

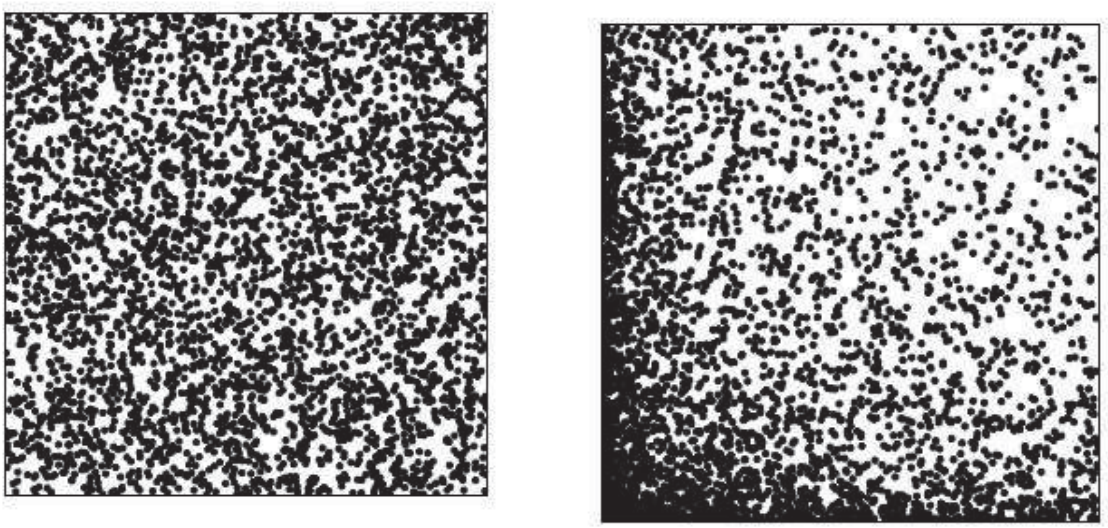

(a) (b)

Figure 3.4: Statistically (a) homogeneous, (b) inhomogeneous microstructures [32].

distribution displays observable and measurable variation and the microstructure exhibits statistical inhomogeneity. Furthermore, the volume fraction of the particles are varies througthout the sample as is shown in Fig.3.4b. In both cases, 64^2 particles distributed all over the sample randomly.

3.3 Testing procedure

Based on the Hill's condition in Eq.3.3 the macro/micro criterion used in effective property calculations [33]

$$\langle \boldsymbol{\sigma} : \boldsymbol{\varepsilon} \rangle_\Omega = \langle \boldsymbol{\sigma} \rangle_\Omega : \langle \boldsymbol{\varepsilon} \rangle_\Omega \tag{3.3}$$

In the absence of body force the Hill's condition were satisfied by two main loading states. They are

1. Pure linear displacements of the form :

$$\mathbf{u}|_{\partial\Omega} = \xi.\mathbf{x} \;\Rightarrow\; \langle \boldsymbol{\varepsilon} \rangle_\Omega = \xi \tag{3.4}$$

2. Pure tractions of the form:

$$\mathbf{t}|_{\partial\Omega} = L.\mathbf{n} \;\Rightarrow\; \langle\boldsymbol{\sigma}\rangle_\Omega = L \tag{3.5}$$

where the ξ and L are the constant strain and stress tensors, respectively. In order to compute the effective constitutive tensor $\mathbf{E}^\star$ a testing procedure will be formulated. The constitutive tensor $\mathbf{E}^\star$ provides the properties of heterogeneous material and the components of the $\mathbf{E}^\star$ tensor are derived by the relation between the average strain and stress tensor

$$\langle\boldsymbol{\sigma}\rangle_\Omega = \mathbf{E}^\star : \langle\boldsymbol{\varepsilon}\rangle_\Omega \tag{3.6}$$

where

$$\langle\cdot\rangle = \frac{1}{|\Omega|}\int_\Omega \cdot\, d\Omega \tag{3.7}$$

and where $\boldsymbol{\sigma}$ and $\boldsymbol{\varepsilon}$ are the stress and strain tensor fields within a microscopic sample of material, with volume $|\Omega|$.
In order to compute the properties of microheterogeneous material,one computes 36 constitutive constants E^*_{ijkl}, in the following relation between the average of strain and stress tensor [33]

$$\begin{Bmatrix} \langle\boldsymbol{\sigma}_{11}\rangle_\Omega \\ \langle\boldsymbol{\sigma}_{22}\rangle_\Omega \\ \langle\boldsymbol{\sigma}_{33}\rangle_\Omega \\ \langle\boldsymbol{\sigma}_{12}\rangle_\Omega \\ \langle\boldsymbol{\sigma}_{13}\rangle_\Omega \\ \langle\boldsymbol{\sigma}_{23}\rangle_\Omega \end{Bmatrix} = \begin{bmatrix} E^*_{1111} & E^*_{1122} & E^*_{1133} & E^*_{1112} & E^*_{1113} & E^*_{1123} \\ E^*_{2211} & E^*_{2222} & E^*_{2233} & E^*_{2212} & E^*_{2213} & E^*_{2223} \\ E^*_{3311} & E^*_{3322} & E^*_{3333} & E^*_{3312} & E^*_{3313} & E^*_{3323} \\ E^*_{1211} & E^*_{1222} & E^*_{1233} & E^*_{1212} & E^*_{1213} & E^*_{1223} \\ E^*_{1311} & E^*_{1322} & E^*_{1333} & E^*_{1312} & E^*_{1313} & E^*_{1323} \\ E^*_{2311} & E^*_{2322} & E^*_{2333} & E^*_{2312} & E^*_{2313} & E^*_{2323} \end{bmatrix} \begin{Bmatrix} \langle\boldsymbol{\varepsilon}_{11}\rangle_\Omega \\ \langle\boldsymbol{\varepsilon}_{22}\rangle_\Omega \\ \langle\boldsymbol{\varepsilon}_{33}\rangle_\Omega \\ 2\langle\boldsymbol{\varepsilon}_{12}\rangle_\Omega \\ 2\langle\boldsymbol{\varepsilon}_{13}\rangle_\Omega \\ 2\langle\boldsymbol{\varepsilon}_{23}\rangle_\Omega \end{Bmatrix} \tag{3.8}$$

We have 6 linear independent load case according to different directions, it can be written,

$$\xi \; or \; L = \begin{bmatrix} \beta & 0 & 0 \\ 0 & 0 & 0 \\ 0 & 0 & 0 \end{bmatrix} \;,\; in\; X\; direction \tag{3.9}$$

$$\xi \; or \; L = \begin{bmatrix} 0 & 0 & 0 \\ 0 & \beta & 0 \\ 0 & 0 & 0 \end{bmatrix} \; , \; in \, Y \; direction \tag{3.10}$$

$$\xi \; or \; L = \begin{bmatrix} 0 & 0 & 0 \\ 0 & 0 & 0 \\ 0 & 0 & \beta \end{bmatrix} \; , \; in \, Z \; direction \tag{3.11}$$

$$\xi \; or \; L = \begin{bmatrix} 0 & \beta & 0 \\ \beta & 0 & 0 \\ 0 & 0 & 0 \end{bmatrix} \; , \; shear \; in \; XY plane \tag{3.12}$$

$$\xi \; or \; L = \begin{bmatrix} 0 & 0 & 0 \\ 0 & 0 & \beta \\ 0 & \beta & 0 \end{bmatrix} \; , \; shear \; in \; ZY plane \tag{3.13}$$

$$\xi \; or \; L = \begin{bmatrix} 0 & 0 & \beta \\ 0 & 0 & 0 \\ \beta & 0 & 0 \end{bmatrix} \; , \; shear \; in \; ZX plane \tag{3.14}$$

Where β is load parameter. It should be mentioned that each independent loading state provide 6 equations, for a total of 36 which are use to calculate the material matrix that is the relation between average strain and stress.

3.3.1 The average strain theorem

Fig.3.5 shows the heterogeneous body has the fowllowing uniform loading on its surface: $\mathbf{u}|_{\partial\Omega} = \xi.\mathbf{x}$, then [33]

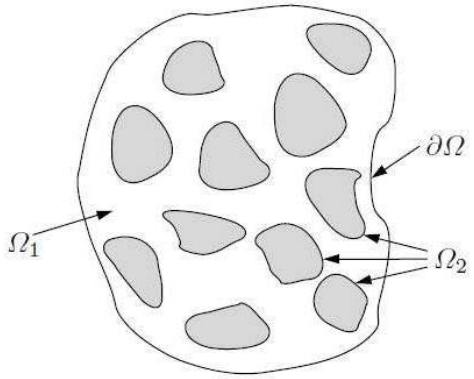

Figure 3.5: Nomenclature for the average theorems [33].

$$
\begin{aligned}
\langle \boldsymbol{\varepsilon} \rangle_\Omega &= \frac{1}{2\,|\Omega|} \int_\Omega \left(\bigtriangledown \mathbf{u} + (\bigtriangledown \mathbf{u})^T \right) d\Omega \\
&= \frac{1}{2\,|\Omega|} \left\{ \int_{\Omega_1} \left(\bigtriangledown \mathbf{u} + (\bigtriangledown \mathbf{u})^T \right) d\Omega + \int_{\Omega_2} \left(\bigtriangledown \mathbf{u} + (\bigtriangledown \mathbf{u})^T \right) d\Omega \right\} \\
&= \frac{1}{2\,|\Omega|} \left\{ \int_{\partial\Omega_1} (\mathbf{u} \otimes \mathbf{n} + \mathbf{n} \otimes \mathbf{u})\, dA + \int_{\partial\Omega_2} (\mathbf{u} \otimes \mathbf{n} + \mathbf{n} \otimes \mathbf{u})\, dA \right\} \\
&= \frac{1}{|2\Omega|} \left\{ \int_{\partial\Omega} ((\xi.\mathbf{x}) \otimes \mathbf{n} + \mathbf{n} \otimes (\xi.\mathbf{x}))\, dA + \int_{\partial\Omega_1 \cap \partial\Omega_2} (\|\mathbf{u}\| \otimes \mathbf{n} + \mathbf{n} \otimes \|\mathbf{u}\|)\, dA \right\} \\
&= \frac{1}{2\,|\Omega|} \left\{ \int_\Omega \left(\bigtriangledown (\xi.\mathbf{x}) + \bigtriangledown (\xi.\mathbf{x})^T \right) d\Omega + \int_{\partial\Omega_1 \cap \partial\Omega_2} (\|\mathbf{u}\| \otimes \mathbf{n} + \mathbf{n} \otimes \|\mathbf{u}\|)\, dA \right\} \\
&= \xi + \frac{1}{2\,|\Omega|} \int_{\partial\Omega_1 \cap \partial\Omega_2} (\|\mathbf{u}\| \otimes \mathbf{n} + \mathbf{n} \otimes \|\mathbf{u}\|)\, dA
\end{aligned}
\tag{3.15}
$$

where $(\mathbf{u} \otimes \mathbf{n} = u_i n_j)$ is the tensor product of the tensor $\mathbf{u}$ and vector $\mathbf{n}$. $\|\mathbf{u}\|$ describes the displacement jumps at the interfaces between Ω_1 and Ω_2. Furthermore, for the perfectly bonded material,

$$
\langle \boldsymbol{\varepsilon} \rangle_\Omega = \xi \tag{3.16}
$$

3.3.2 The average stress theorem

In this case we consider the heterogeneous body with $\mathbf{t}|_{\partial\Omega} = L.\mathbf{n}$. By using the identity $\bigtriangledown.(\boldsymbol{\sigma} \otimes \mathbf{x}) = (\bigtriangledown.\boldsymbol{\sigma}) \otimes \mathbf{x} + \boldsymbol{\sigma}.\bigtriangledown \mathbf{x} = -\mathbf{f} \otimes \boldsymbol{x} + \boldsymbol{\sigma}$ and substitute this into the definition of the average stress

$$\begin{aligned}
\langle \boldsymbol{\sigma} \rangle_\Omega &= \frac{1}{|\Omega|} \int_\Omega \bigtriangledown.(\boldsymbol{\sigma} \otimes \mathbf{x})\, d\Omega + \frac{1}{|\Omega|} \int_\Omega (\boldsymbol{f} \otimes \mathbf{x})\, d\Omega \\
&= \frac{1}{|\Omega|} \int_{\partial\Omega} (\boldsymbol{\sigma} \otimes \mathbf{x}).\mathbf{n} dA + \frac{1}{|\Omega|} \int_\Omega (\boldsymbol{f} \otimes \mathbf{x})\, dA \\
&= \frac{1}{|\Omega|} \int_{\partial\Omega} (L \otimes \mathbf{x}).\mathbf{n} dA + \frac{1}{|\Omega|} \int_\Omega (\boldsymbol{f} \otimes \mathbf{x})\, dA \\
&= L + \frac{1}{|\Omega|} \int_\Omega (\boldsymbol{f} \otimes \mathbf{x})\, dA
\end{aligned} \tag{3.17}$$

If there is no body force $\boldsymbol{f} = 0$, then

$$\langle \boldsymbol{\sigma} \rangle_\Omega = L \tag{3.18}$$

Note that considering the interface separation (debonding) has not any effect on the result.

3.4 Homogenization Methods

3.4.1 Analytical Methods

Mori-Tanaka Method

The assumption of non-interaction of particulates is an unreasonable expectation for materials which spread in different directions over a volume fraction. Considering of week interaction between particles by sensitivity make a minor alternation to the dilute method. It is noticeable that for spherical inclusion the Mori-Tanaka method provid-

ing the suitable effective properties matches the Hashin-Shtrikman lower bound. The effective bulk and shear modules is given by [33],

$$\begin{aligned} k^* &= \kappa_1 + \upsilon_2 (\kappa_2 - \kappa_1) \eta \\ \mu^* &= \mu_1 + \nu_2 (\mu_2 - \mu_1) \zeta \end{aligned} \tag{3.19}$$

where, κ_1 and μ_1 are the bulk and shear moduli of the matrix, κ_2 and μ_2 are the bulk and shear moduli of the inclusion, ν_2 is the volume fraction of inclusion. According to the Eq.3.19 k^* is the effective bulk modulus and μ^* is the effective shear modulus, where

$$\begin{aligned} \phi &= \mu_1 + \frac{\mu_1 (9\kappa_1 + 8\mu_1)}{6 (\kappa_1 + 2\mu_1)} \\ \Theta &= \kappa_1 + \frac{4}{3}\mu_1 \\ \zeta &= \frac{\phi}{\phi + (1 - \nu_2)(\mu_2 - \mu_1)} \\ \eta &= \frac{\Theta}{\Theta + (1 - \nu_2)(\kappa_2 - \kappa_1)} \end{aligned} \tag{3.20}$$

Dilute Method

According to Eshelby [34] results which means the resulting strain field inside the inclusion is uniform, it is simple as a method of determining the effective material properties for shaped particles. Furthermore, dilute approximation only apply to extremely low volume fraction of the heterogeneous materials. We have [33],

$$\begin{aligned} k^* &= \kappa_1 + \nu_2 (\kappa_2 - \kappa_1) \gamma \\ \mu^* &= \mu_1 + \nu_2 (\mu_2 - \mu_1) \rho \end{aligned} \tag{3.21}$$

where

$$\begin{aligned}\alpha &= \frac{3\kappa_1}{3\kappa_1 + 4\mu_1} \\ \beta &= \frac{6}{5}\frac{\kappa_1 + 2\mu_1}{3\kappa_1 + 4\mu_1} \\ \gamma &= \frac{\kappa_1}{\alpha\kappa_2 + \kappa_1(1-\alpha)} \\ \rho &= \frac{\mu_1}{\beta\mu_2 + \mu_1(1-\beta)}\end{aligned} \tag{3.22}$$

The Asymptotic Hashin-Shtrikman Bounds Method

According to the concept of polarization or filtering of micro-macro mechanical fields the bounds were developed by Hashin and Shtrikman [35, 36]. These bounds depend on certain factors such as sample size which means when the sample size goes to infinity size in relation to the micro constituent length scale, they are valuable. In this case we obtain,

$$\begin{aligned}k^{*,-} &= \kappa_1 + \frac{\nu_2}{\left(\frac{1}{\kappa_2-\kappa_1} + \frac{3(1-\nu_2)}{3\kappa_1+4\mu_1}\right)} \\ k^{*,+} &= \kappa_2 + \frac{1-\nu_2}{\left(\frac{1}{\kappa_1-\kappa_2} + \frac{3\nu_2}{3\kappa_2+4\mu_2}\right)} \\ \mu^{*,-} &= \mu_1 + \frac{\nu_2}{\left(\frac{1}{\mu_2-\mu_1} + \frac{6(1-\nu_2)(\kappa_1+2\mu_1)}{5\mu_1(3\kappa_1+4\mu_1)}\right)} \\ \mu^{*,+} &= \mu_2 + \frac{1-\nu_2}{\left(\frac{1}{\mu_1-\mu_2} + \frac{6\nu_2(\kappa_2+2\mu_2)}{5\mu_2(3\kappa_2+4\mu_2)}\right)}\end{aligned} \tag{3.23}$$

where, $k^{*,-}$ and $k^{*,+}$ are the bulk modulus H-S lower bound and the bulk modulus H-S upper bound, respectively. In addition $\mu^{*,-}$ and $\mu^{*,+}$ are the shear modulus H-S lower bound and the shear modulus H-S upper bound respectively.

Reuss Method

The assumption of uniform (constant) stress field within a sample of aggregate of polycrystalline material under applying exterior uniform stress (uniform traction boundary condition) was introduced by Reuss [37] in 1929, where ε is a constant and $\nu_1 + \nu_2 = 1$, where the ν_2 as a volume fraction of inclusion and ν_1 is volume fraction of matrix.

$$\begin{aligned} k^* &= \frac{\kappa_1 \kappa_2}{\kappa_2 (1 - \nu_2) + \kappa_1 \nu_2} \\ \mu^* &= \frac{\mu_1 \mu_2}{\mu_2 (1 - \nu_2) + \mu_1 \nu_2} \end{aligned} \tag{3.24}$$

Voigt Method

The assumption of uniform (constant) strain field within a sample of aggregate of polycrystalline material under applying exterior uniform strain (linear displacement boundary condition) was introduced by Voigt [38] in 1889, where σ is constant and $\nu_1 + \nu_2 = 1$, where the ν_2 as a volume fraction of inclusion and ν_1 is volume fraction of matrix.

$$\begin{aligned} k^* &= (1 - \nu_2) \kappa_1 + \nu_2 \kappa_2 \\ \mu^* &= (1 - \nu_2) \mu_1 + \nu_2 \mu_2 \end{aligned} \tag{3.25}$$

Self Consistent Method

The Self Consistent method [33] which is used to consolidate particulate interaction and it's another approach which is equal to dilute approximation. It should be noted that this method make a logical results only for low volume fraction. The effective bulk and shear modules is given by,

$$\begin{aligned} k^* &= \kappa_1 \left(1 - \nu_2 \frac{\gamma - 1}{\alpha} \right) \\ \mu^* &= \mu_1 \left(1 - \nu_2 \frac{\rho - 1}{\beta} \right) \end{aligned} \tag{3.26}$$

Mori-Tanaka method (without interphase layer)

The Mori-Tanaka method [9, 10] was used to determine the elastic properties of two-phase composites (matrix and inclusion). The overall elastic stiffness tensor of composite is [8]

$$\mathbf{C} = \left(\nu_1 \mathbf{C}^m + \nu_2 \mathbf{C}^p \mathbf{T}^p\right) \left(\nu_1 \mathbf{I} + \nu_2 \mathbf{T}^p\right)^{-1} \tag{3.27}$$

where ν_1 and ν_2 are the volume fraction of matrix and particle, $\mathbf{C}^m$ and $\mathbf{C}^p$ are the stiffness tensor of the matrix and particle, $\mathbf{I}$ is the identity tensor and $\mathbf{T}^p$ is dilute strain-concentration tensor of the effective particle,

$$\mathbf{T}^p = \left[\mathbf{I} + \mathbf{S}^p \left(\mathbf{C}^m\right)^{-1} \left(\mathbf{C}^p - \mathbf{C}^m\right)\right]^{-1} \tag{3.28}$$

where $\mathbf{S}^p$ is the Eshelby tensor [34]. For spherical particle within an isotropic matrix, the components of Eshelby tensor can be written as [39]

$$\begin{aligned} S_{1111} &= S_{2222} = S_{3333} = \frac{7 - 5\nu}{15\left(1 - \nu\right)} \\ S_{1122} &= S_{2233} = S_{3311} = S_{1133} = S_{2211} = S_{3322} = \frac{5\nu - 1}{15\left(1 - \nu\right)} \\ S_{1212} &= S_{2323} = S_{3131} = \frac{4 - 5\nu}{15\left(1 - \nu\right)} \end{aligned} \tag{3.29}$$

where ν is the poisson's ratio of matrix. The components of the Eshelby tensor for cylindrical fiber within an isotropic matrix, can be also written [40]

$$\begin{aligned}
S_{1111} &= \frac{1}{2(1-\nu)}\left[\frac{b^2+2ab}{(a+b)^2}+(1-2\nu)\frac{b}{a+b}\right] \\
S_{2222} &= \frac{1}{2(1-\nu)}\left[\frac{a^2+2ab}{(a+b)^2}+(1-2\nu)\frac{a}{a+b}\right] \\
S_{3333} &= 0 \\
S_{1122} &= \frac{1}{2(1-\nu)}\left[\frac{b^2}{(a+b)^2}-(1-2\nu)\frac{b}{a+b}\right] \\
S_{2233} &= \frac{1}{2(1-\nu)}\frac{2\nu a}{a+b} \\
S_{2211} &= \frac{1}{2(1-\nu)}\left[\frac{a^2}{(a+b)^2}-(1-2\nu)\frac{a}{a+b}\right] \\
S_{3311} &= S_{3322} = 0 \\
S_{1212} &= \frac{1}{2(1-\nu)}\left[\frac{a^2+b^2}{2(a+b)^2}+\frac{(1-2\nu)}{2}\right] \\
S_{1133} &= \frac{1}{2(1-\nu)}\frac{2\nu a}{a+b} \\
S_{2323} &= \frac{a}{2(a+b)} \\
S_{3131} &= \frac{b}{2(a+b)}
\end{aligned} \tag{3.30}$$

where a=b are equal to the radius of inclusion.

Mori-Tanaka method (with interphase layer)

Dunn and Ledbetter [41] developed the effective interface model for composites with two phase particles (inclusion and interphase zone) to predict the overall elastic stiffness tensor of the composite is

$$\mathbf{C} = \mathbf{C}^m + \left[(\nu_2+\nu_i)\left(\mathbf{C}^i-\mathbf{C}^m\right)\mathbf{T}^{pi}+\nu_2\left(\mathbf{C}^p-\mathbf{C}^i\right)\mathbf{T}^p\right]\times\left[\nu_1\mathbf{I}+(\nu_2+\nu_i)\,\mathbf{T}^{pi}\right]^{-1} \tag{3.31}$$

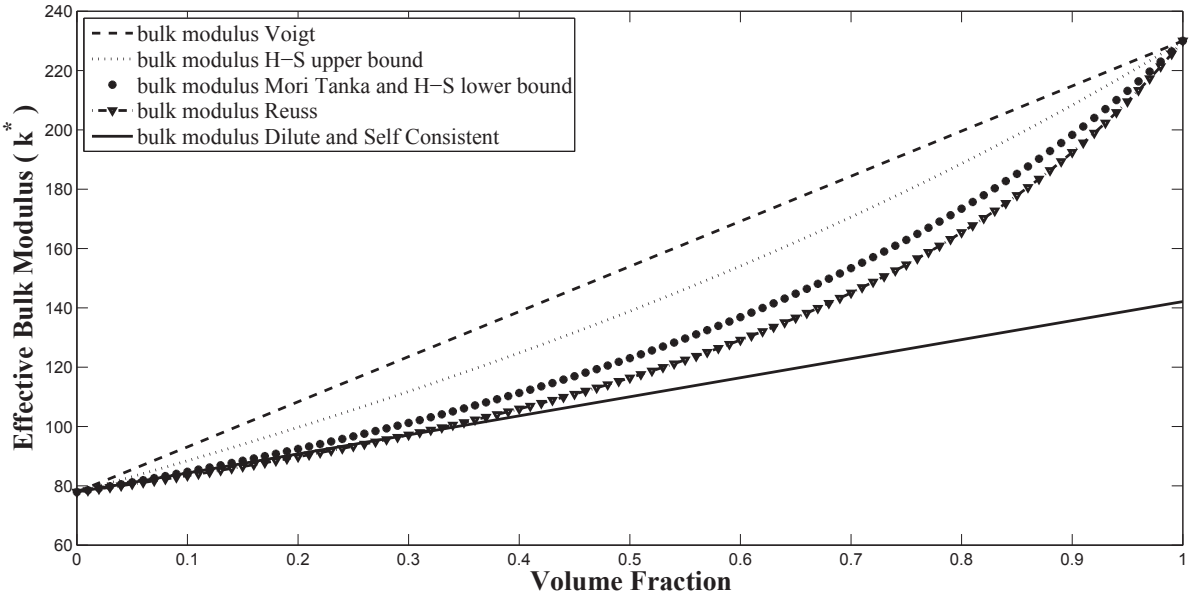

Figure 3.6: The Predictive Effective Bulk Modulus k^* for an Aluminum matrix and Boron particle

where ν_i is the effective volume fraction of interface, $\mathbf{C}^i$ is the stiffness tensor for interface and $\mathbf{T}^p$ and $\mathbf{T}^{pi}$ are the dilute strain-concentration tensors for the particle and interphase given by,

$$\begin{aligned}
\mathbf{T}^p &= \mathbf{I} - \mathbf{S}^p \left[\mathbf{S}^p + \left(\mathbf{C}^p - \mathbf{C}^m\right)^{-1} \mathbf{C}^m\right]^{-1} \\
\mathbf{T}^{pi} &= \mathbf{I} - \mathbf{S}^p \left\{ \frac{\nu_2}{\nu_i + \nu_2} \left[\mathbf{S}^p + \left(\mathbf{C}^p - \mathbf{C}^m\right)^{-1} \mathbf{C}^m\right]^{-1} + \frac{\nu_i}{\nu_i + \nu_2} \left[\mathbf{S}^p + \left(\mathbf{C}^i - \mathbf{C}^m\right)^{-1} \mathbf{C}^m\right]^{-1} \right\}
\end{aligned} \tag{3.32}$$

In this study, we consider aluminum and boron as matrix ($\kappa_1 = 77.9GPa$, $\mu_1 = 24.9GPa$) and particle ($\kappa_2 = 230GPa$, $\mu_2 = 172GPa$), respectively. This information was used to calculate the effective bulk modulus (k^*) and the effective shear modulus (μ^*). As seen in Fig.3.6 and 3.7.

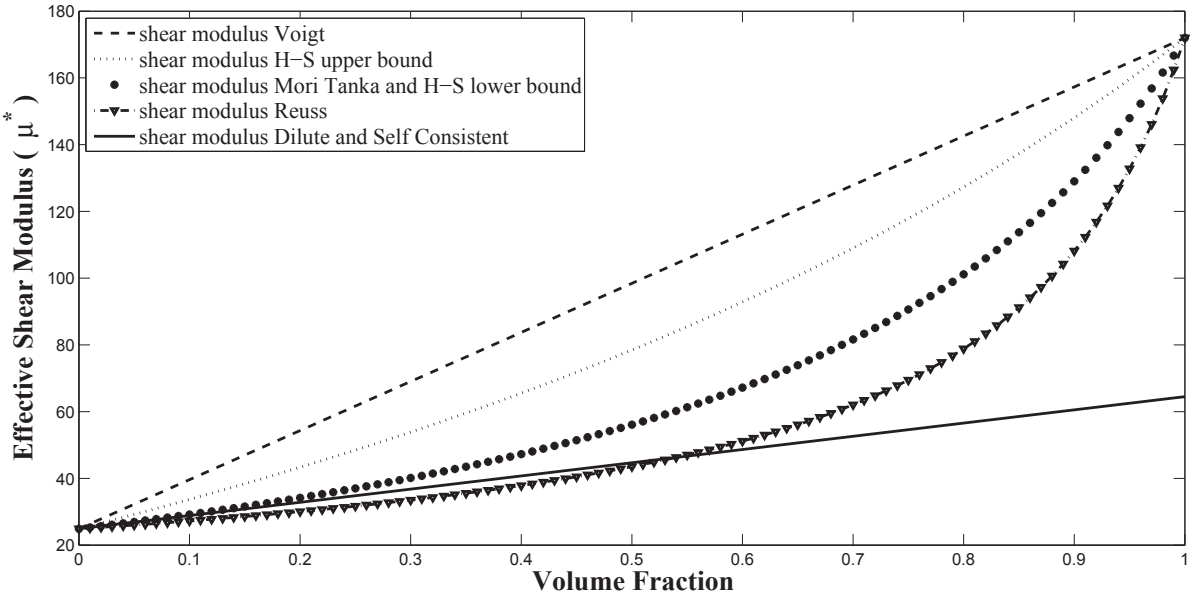

Figure 3.7: The Predictive Effective Shear Modulus μ^* for an Aluminum matrix and Boron particle

3.4.2 Finite Element method

Linear elasticity-3D

Under general conditions with a linear elastic law, we have

$$\begin{bmatrix} \sigma_{11} \\ \sigma_{22} \\ \sigma_{33} \\ \tau_{12} \\ \tau_{13} \\ \tau_{23} \end{bmatrix} = \begin{bmatrix} D_{1111} & D_{1122} & D_{1133} & D_{1112} & D_{1113} & D_{1123} \\ D_{1122} & D_{2222} & D_{2233} & D_{2212} & D_{2213} & D_{2223} \\ D_{1133} & D_{2233} & D_{3333} & D_{3312} & D_{3313} & D_{3323} \\ D_{1112} & D_{2212} & D_{3312} & D_{1212} & D_{1213} & D_{1223} \\ D_{1113} & D_{2213} & D_{3313} & D_{1213} & D_{1313} & D_{1323} \\ D_{1123} & D_{2223} & D_{3323} & D_{1223} & D_{1323} & D_{2323} \end{bmatrix} \begin{bmatrix} \varepsilon_{11} \\ \varepsilon_{22} \\ \varepsilon_{33} \\ \gamma_{12} \\ \gamma_{13} \\ \gamma_{23} \end{bmatrix} \tag{3.33}$$

Hooke's law for isotropic material can be written as,

$$\begin{bmatrix}\sigma_{11}\\ \sigma_{22}\\ \sigma_{33}\\ \sigma_{12}\\ \sigma_{13}\\ \sigma_{23}\end{bmatrix} = \begin{bmatrix}\lambda+2\mu & \lambda & \lambda & 0 & 0 & 0\\ \lambda & \lambda+2\mu & \lambda & 0 & 0 & 0\\ \lambda & \lambda & \lambda+2\mu & 0 & 0 & 0\\ 0 & 0 & 0 & \mu & 0 & 0\\ 0 & 0 & 0 & 0 & \mu & 0\\ 0 & 0 & 0 & 0 & 0 & \mu\end{bmatrix} \begin{bmatrix}\varepsilon_{11}\\ \varepsilon_{22}\\ \varepsilon_{33}\\ 2\varepsilon_{12}\\ 2\varepsilon_{13}\\ 2\varepsilon_{23}\end{bmatrix} \tag{3.34}$$

Where, E is Young's modulus and ν is Poisson's ratio,

$$\lambda = \frac{\nu E}{(1+\nu)(1-2\nu)} \tag{3.35}$$

and

$$\mu = \frac{E}{2(1+\nu)} \tag{3.36}$$

The inverse of relation can be written as,

$$\begin{bmatrix}\varepsilon_{11}\\ \varepsilon_{22}\\ \varepsilon_{33}\\ \gamma_{12}\\ \gamma_{13}\\ \gamma_{23}\end{bmatrix} = \begin{bmatrix}\varepsilon_{11}\\ \varepsilon_{22}\\ \varepsilon_{33}\\ 2\varepsilon_{12}\\ 2\varepsilon_{13}\\ 2\varepsilon_{23}\end{bmatrix} = \frac{1}{E}\begin{bmatrix}1 & -\nu & -\nu & 0 & 0 & 0\\ -\nu & 1 & -\nu & 0 & 0 & 0\\ -\nu & -\nu & 1 & 0 & 0 & 0\\ 0 & 0 & 0 & 2(1+\nu) & 0 & 0\\ 0 & 0 & 0 & 0 & 2(1+\nu) & 0\\ 0 & 0 & 0 & 0 & 0 & 2(1+\nu)\end{bmatrix} \begin{bmatrix}\sigma_{11}\\ \sigma_{22}\\ \sigma_{33}\\ \sigma_{12}\\ \sigma_{13}\\ \sigma_{23}\end{bmatrix} \tag{3.37}$$

Where, γ is shear strain.($\gamma_{ij} = 2\varepsilon_{ij}$)

In the case of material constitutive models for orthotropic material ,it should be clear that there are 9 independent components to elasticity matrix along 3 directions.In other words, we have 3 young's moduli (E_1, E_2, E_3), 3 shear moduli (G_{12}, G_{13}, G_{23})and

3 poisson's ratios (ν_{12}, ν_{23}, ν_{13}).

$$\begin{bmatrix} \sigma_{11} \\ \sigma_{22} \\ \sigma_{33} \\ \tau_{12} \\ \tau_{13} \\ \tau_{23} \end{bmatrix} = \begin{bmatrix} D_{1111} & D_{1122} & D_{1133} & 0 & 0 & 0 \\ D_{1122} & D_{2222} & D_{2233} & 0 & 0 & 0 \\ D_{1133} & D_{2233} & D_{3333} & 0 & 0 & 0 \\ 0 & 0 & 0 & D_{1212} & 0 & 0 \\ 0 & 0 & 0 & 0 & D_{1313} & 0 \\ 0 & 0 & 0 & 0 & 0 & D_{2323} \end{bmatrix} \begin{bmatrix} \varepsilon_{11} \\ \varepsilon_{22} \\ \varepsilon_{33} \\ \gamma_{12} \\ \gamma_{13} \\ \gamma_{23} \end{bmatrix} \tag{3.38}$$

The fourth order tensor can be represented as $\sigma_{ij} = C_{ijkl}\varepsilon_{kl}$,in addition converting tensor according to Voigt notation reduced to second order as $\sigma_i = C_{ij}\varepsilon_j$.

$$C = \begin{bmatrix} D_{1111} & D_{1122} & D_{1133} & 0 & 0 & 0 \\ D_{1122} & D_{2222} & D_{2233} & 0 & 0 & 0 \\ D_{1133} & D_{2233} & D_{3333} & 0 & 0 & 0 \\ 0 & 0 & 0 & D_{1212} & 0 & 0 \\ 0 & 0 & 0 & 0 & D_{1313} & 0 \\ 0 & 0 & 0 & 0 & 0 & D_{2323} \end{bmatrix} \tag{3.39}$$

With considering Voigt notation,

$$C = \begin{bmatrix} D_{11} & D_{12} & D_{13} & 0 & 0 & 0 \\ D_{12} & D_{22} & D_{23} & 0 & 0 & 0 \\ D_{13} & D_{23} & D_{33} & 0 & 0 & 0 \\ 0 & 0 & 0 & D_{44} & 0 & 0 \\ 0 & 0 & 0 & 0 & D_{55} & 0 \\ 0 & 0 & 0 & 0 & 0 & D_{66} \end{bmatrix} \tag{3.40}$$

Where, C is the stiffness matrix .The components of stiffness tensor of orthotropic ma-

terial calculated by using the following formulae,

$$\begin{aligned}
D_{1111} &= E_1 \left(1 - \nu_{23}\nu_{32}\right) \Upsilon \\
D_{2222} &= E_2 \left(1 - \nu_{13}\nu_{31}\right) \Upsilon \\
D_{3333} &= E_3 \left(1 - \nu_{12}\nu_{21}\right) \Upsilon \\
D_{1122} &= E_1 \left(\nu_{21} - \nu_{31}\nu_{23}\right) \Upsilon = E_2 \left(\nu_{12} - \nu_{32}\nu_{13}\right) \Upsilon \\
D_{1133} &= E_1 \left(\nu_{31} - \nu_{21}\nu_{32}\right) \Upsilon = E_3 \left(\nu_{13} - \nu_{12}\nu_{23}\right) \Upsilon \\
D_{2233} &= E_2 \left(\nu_{32} - \nu_{12}\nu_{31}\right) \Upsilon = E_3 \left(\nu_{23} - \nu_{21}\nu_{13}\right) \Upsilon \\
D_{1212} &= G_{12} \\
D_{1313} &= G_{13} \\
D_{2323} &= G_{23} \\
\Upsilon &= \frac{1}{1 - \nu_{12}\nu_{21} - \nu_{23}\nu_{32} - \nu_{31}\nu_{13} - 2\nu_{21}\nu_{32}\nu_{13}}
\end{aligned} \tag{3.41}$$

Material stability requires to obey these criteria,

$$\begin{aligned}
E_1, E_2, E_3, G_{12}, G_{13}, G_{23} &> 0 \\
|\nu_{12}| &< \left(E_1/E_2\right)^{1/2} \\
|\nu_{13}| &< \left(E_1/E_3\right)^{1/2} \\
|\nu_{23}| &< \left(E_2/E_3\right)^{1/2} \\
1 - \nu_{12}\nu_{21} - \nu_{23}\nu_{32} - \nu_{31}\nu_{13} - 2\nu_{21}\nu_{32}\nu_{13} &> 0
\end{aligned} \tag{3.42}$$

In addition, there are relations between poisson's ratio based on principle direction we may write,

$$\frac{\nu_{ij}}{E_i} = \frac{\nu_{ji}}{E_j} \tag{3.43}$$

Therefore,we must have

$$\begin{aligned}
\frac{\nu_{12}}{E_1} &= \frac{\nu_{21}}{E_2} \\
\frac{\nu_{13}}{E_1} &= \frac{\nu_{31}}{E_3} \\
\frac{\nu_{23}}{E_2} &= \frac{\nu_{32}}{E_3}
\end{aligned} \tag{3.44}$$

The inverse of stiffness matrix is commonly written as

$$\begin{bmatrix} \varepsilon_{11} \\ \varepsilon_{22} \\ \varepsilon_{33} \\ 2\varepsilon_{12} \\ 2\varepsilon_{13} \\ 2\varepsilon_{23} \end{bmatrix} = \begin{bmatrix} \frac{1}{E_1} & -\frac{\nu_{12}}{E_1} & -\frac{\nu_{13}}{E_1} & 0 & 0 & 0 \\ -\frac{\nu_{12}}{E_1} & \frac{1}{E_2} & -\frac{\nu_{23}}{E_2} & 0 & 0 & 0 \\ -\frac{\nu_{13}}{E_1} & -\frac{\nu_{23}}{E_2} & \frac{1}{E_3} & 0 & 0 & 0 \\ 0 & 0 & 0 & \frac{1}{G_{12}} & 0 & 0 \\ 0 & 0 & 0 & 0 & \frac{1}{G_{13}} & 0 \\ 0 & 0 & 0 & 0 & 0 & \frac{1}{G_{23}} \end{bmatrix} \begin{bmatrix} \sigma_{11} \\ \sigma_{22} \\ \sigma_{33} \\ \sigma_{12} \\ \sigma_{13} \\ \sigma_{23} \end{bmatrix} \tag{3.45}$$

The fourth order tensor can be represented as $\varepsilon_{ij} = S_{ijkl}\sigma_{kl}$,in addition converting tensor according to Voigt notation reduced to second order as $\varepsilon_i = S_{ij}\sigma_j$. For illustration of purpose as written,

$$S = \begin{bmatrix} S_{11} & S_{12} & S_{13} & 0 & 0 & 0 \\ S_{12} & S_{22} & S_{23} & 0 & 0 & 0 \\ S_{13} & S_{23} & S_{33} & 0 & 0 & 0 \\ 0 & 0 & 0 & S_{44} & 0 & 0 \\ 0 & 0 & 0 & 0 & S_{55} & 0 \\ 0 & 0 & 0 & 0 & 0 & S_{66} \end{bmatrix} = \begin{bmatrix} \frac{1}{E_1} & -\frac{\nu_{12}}{E_1} & -\frac{\nu_{13}}{E_1} & 0 & 0 & 0 \\ -\frac{\nu_{12}}{E_1} & \frac{1}{E_2} & -\frac{\nu_{23}}{E_2} & 0 & 0 & 0 \\ -\frac{\nu_{13}}{E_1} & -\frac{\nu_{23}}{E_2} & \frac{1}{E_3} & 0 & 0 & 0 \\ 0 & 0 & 0 & \frac{1}{G_{12}} & 0 & 0 \\ 0 & 0 & 0 & 0 & \frac{1}{G_{13}} & 0 \\ 0 & 0 & 0 & 0 & 0 & \frac{1}{G_{23}} \end{bmatrix} \tag{3.46}$$

Where, S is the compliance.

Plane Stress

In the case of isotropic material,under condition of plane stress ,there is a requirement that must be met ,(σ_{33}=σ_{13}=σ_{31}=σ_{23}=σ_{32}=0). In the x-y plane we have,

$$\begin{bmatrix} \varepsilon_{11} \\ \varepsilon_{22} \\ \gamma_{12} \end{bmatrix} = \begin{bmatrix} 1 & -\nu & 0 \\ -\nu & 1 & 0 \\ 0 & 0 & 2\,(1+\nu) \end{bmatrix} \begin{bmatrix} \sigma_{11} \\ \sigma_{22} \\ \tau_{12} \end{bmatrix} \tag{3.47}$$

Where, $\tau_{12} = 2\varepsilon_{12}$. The inverse relation is,

$$\begin{bmatrix} \sigma_1 \\ \sigma_2 \\ \tau_{12} \end{bmatrix} = \frac{E}{1-\nu^2} \begin{bmatrix} 1 & \nu & 0 \\ \nu & 1 & 0 \\ 0 & 0 & \frac{1-\nu}{2} \end{bmatrix} \begin{bmatrix} \varepsilon_1 \\ \varepsilon_2 \\ \gamma_{12} \end{bmatrix} \tag{3.48}$$

In the case of orthotropic material,under condition of plane stress,there is a requirement that must be met ,(σ_{33}=σ_{13}=σ_{23}=0). In the x-y plane we have,

$$\begin{bmatrix} \varepsilon_1 \\ \varepsilon_2 \\ \gamma_{12} \end{bmatrix} = \begin{bmatrix} \frac{1}{E_1} & -\frac{\nu_{12}}{E_1} & 0 \\ -\frac{\nu_{12}}{E_1} & \frac{1}{E_2} & 0 \\ 0 & 0 & \frac{1}{G_{12}} \end{bmatrix} \begin{bmatrix} \sigma_{11} \\ \sigma_{22} \\ \tau_{12} \end{bmatrix} \tag{3.49}$$

Where, $\tau_{12} = 2\varepsilon_{12}$. The inverse relation is,

$$\begin{bmatrix} \sigma_1 \\ \sigma_2 \\ \tau_{12} \end{bmatrix} = \frac{1}{1-\nu_{12}\nu_{21}} \begin{bmatrix} E_1 & \nu_{21}E_1 & 0 \\ \nu_{12}E_2 & E_2 & 0 \\ 0 & 0 & G_{12}\left(1-\nu_{12}\nu_{21}\right) \end{bmatrix} \begin{bmatrix} \varepsilon_1 \\ \varepsilon_2 \\ \gamma_{12} \end{bmatrix} \tag{3.50}$$

In this study, we consider the copper as a matrix (Em) with the Young's modulus of 126.5 GPA and the poisson's ratio of 0.35, whereas these constant for inclusion (Ep) that is diamond are 1148.3 GPA and 0.068 for Yong's modulus and poisson's ratio of the particle, respectively. Furthermore, it was assumed that the Young's modulus and poisson's ratio of interphase are 80 GPA and 0.1, respectively. Note that the thickness of interphase layer is h which is shown in Fig.3.8. We suppose two kinds of geometric particles: sphere and cylinder. Fig.3.9 show the details of RVE with dimensions of 1m*1m*1m. It should be mentioned that radius of sphere and cylinder inclusion are 0.2 m and 0.1 m, respectively. Fig.3.10 shows the comparison between the numerical and analytical results for sphere inclusion. Moreover, in order to obtain a precise bounds, the LD boundary condition (upper bounds) and UT boundary condition (lower bounds) are simulated using FEM models. Since the assumptions of Mori-Tanaka method are based on the spherical shape and fully embedded inclusion, the analytical results are in a very good agreement with numerical results. Fig.3.10a illustrate the normalized homogenized Young's modulus of diomends which reinforced in copper matrix versus

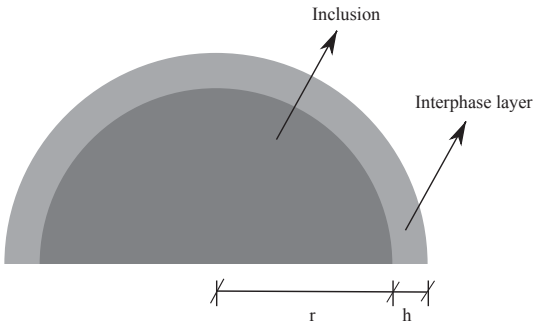

Figure 3.8: The schematic shape of spherical inhomogeneity of radius r with interphase zone of thickness h.

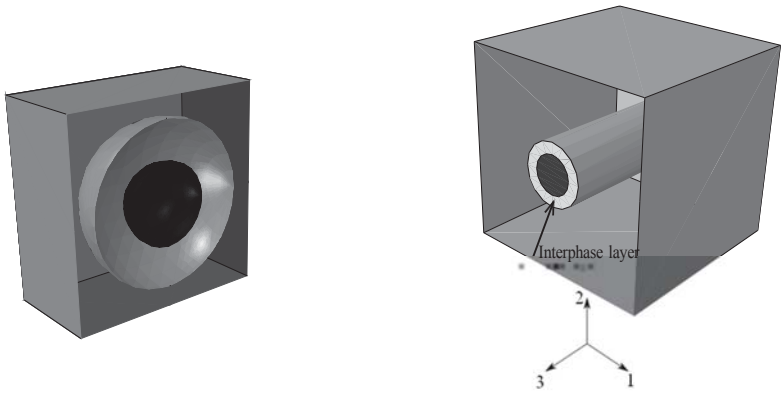

(a) (b)

Figure 3.9: A detailed view of 3D finite element RVE for evaluate the elastic modulus of composite, (a) frame model of sphere with interphase layer , (b) frame model of cylinder with interphase layer .

the change of volume fraction of sphere inclusion. Fig.3.10b demonstrates the effect of interphase layer on the overall elastic modulus of composite, for the constant particle volume fraction of $\nu_2 = 0.0335$. Furthermore, with increasing the thickness of interphase region the homogenized Young's modulus are decreasing. The result of homogenized Young's modulus for cylinder inclusion are shown in Fig.3.11 and Fig.3.12 according to the transverse direction of cylinder and direction of cylinder.

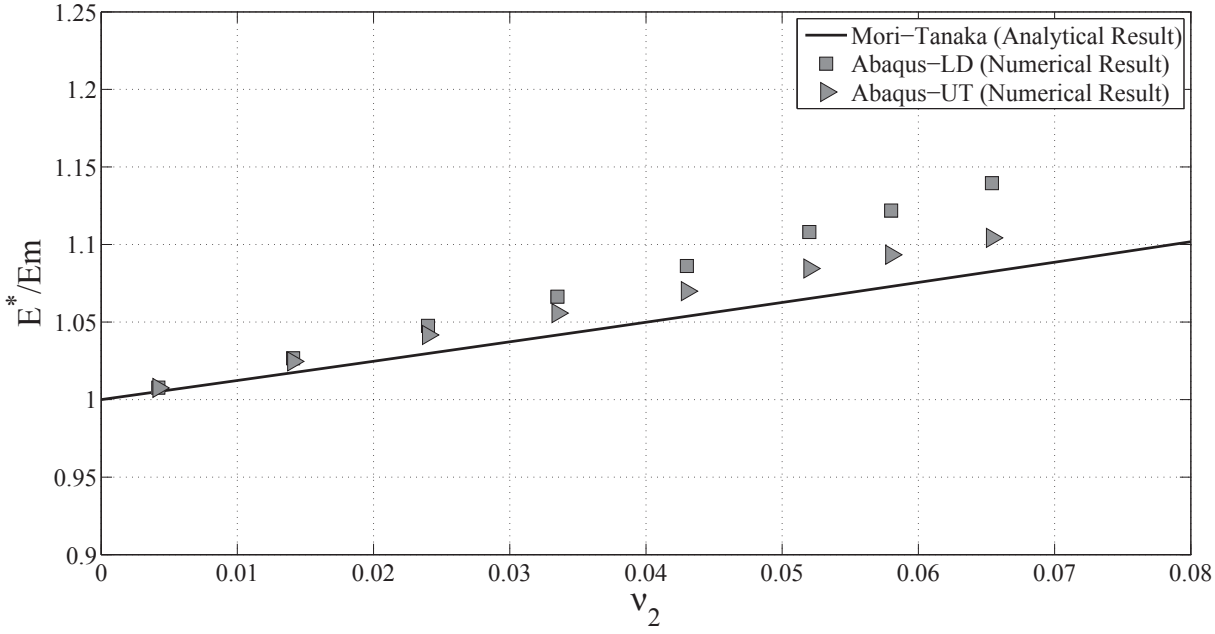

(a)

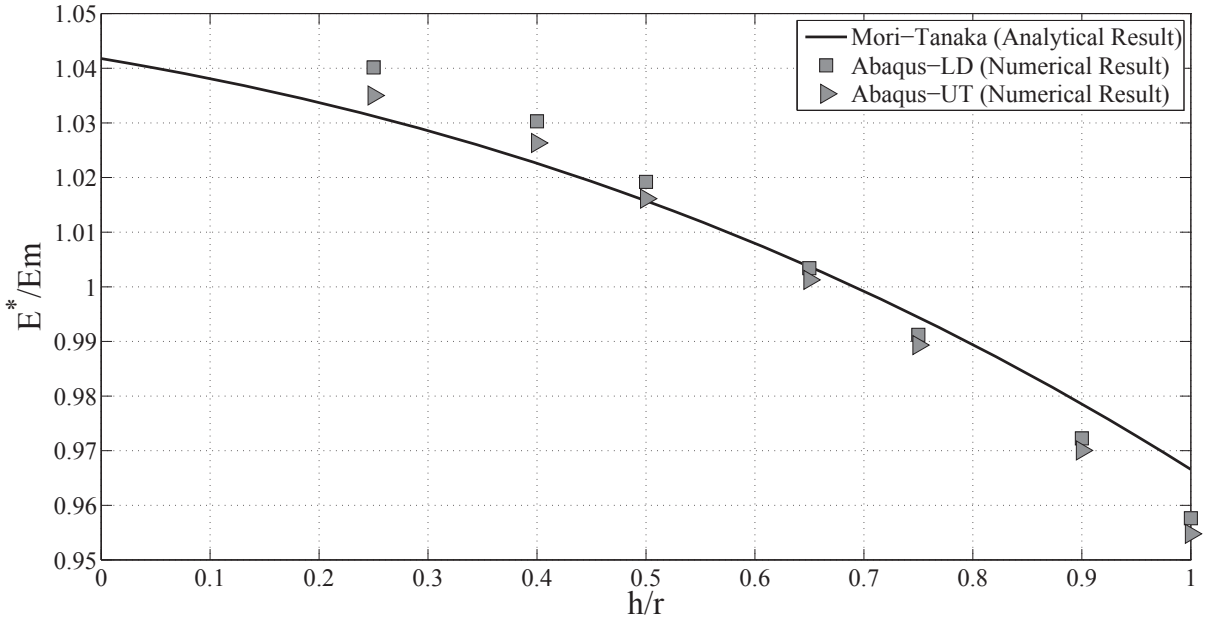

(b)

Figure 3.10: Normalized homogenized Young's modulus (E^*/Em) of diamond reinforced copper matrix vs: (a) volume fraction of sphere inclusion (ν_2), (b) normalized interphase thickness (h/r), for the constant particle volume fraction of $\nu_2 = 0.0335$.

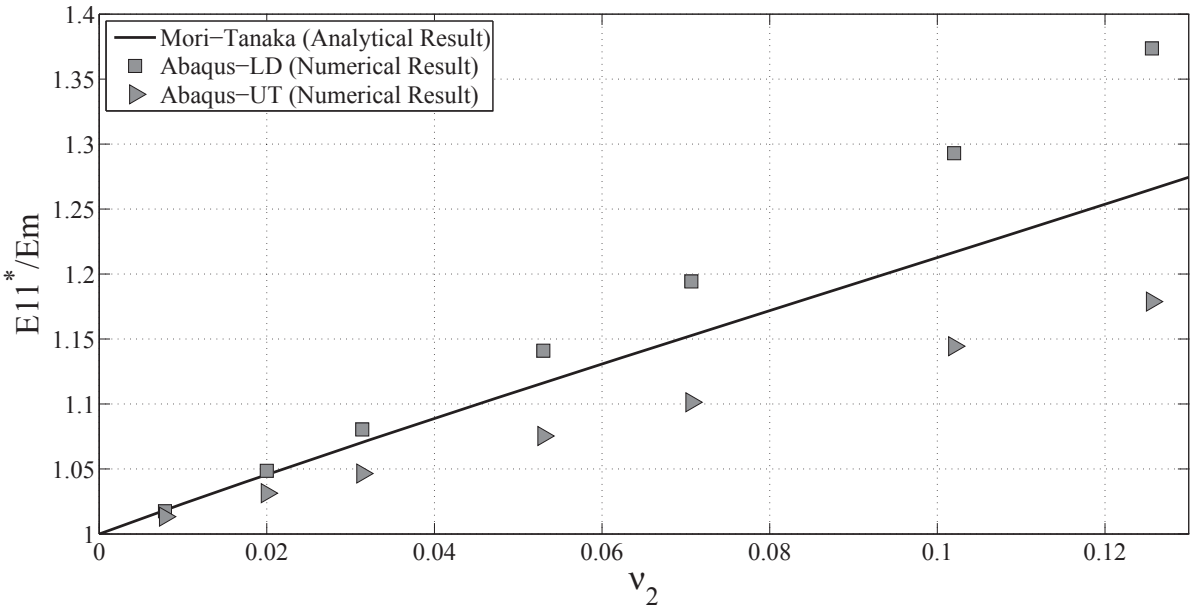

(a)

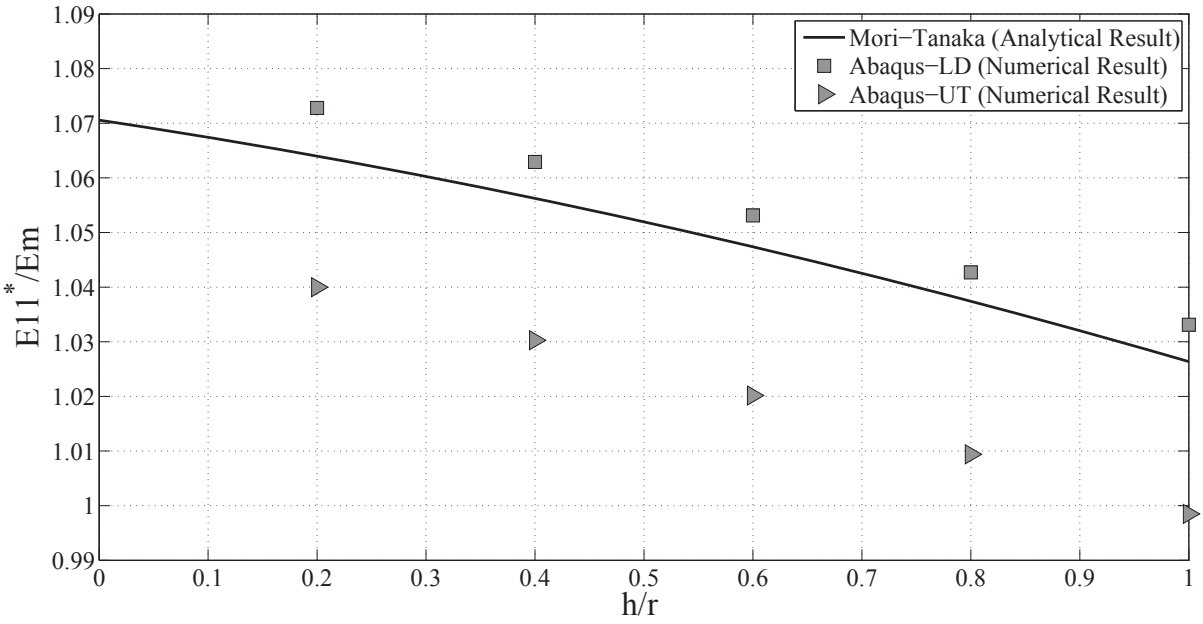

(b)

Figure 3.11: Normalized homogenized Young's modulus ($E11^*$/Em and $E22^*$/Em) of diamond reinforced copper matrix in transverse direction of cylinder vs: (a) volume fraction of cylinder inclusion (ν_2), (b) normalized interphase thickness (h/r), for the constant particle volume fraction of $\nu_2 = 0.0314$.

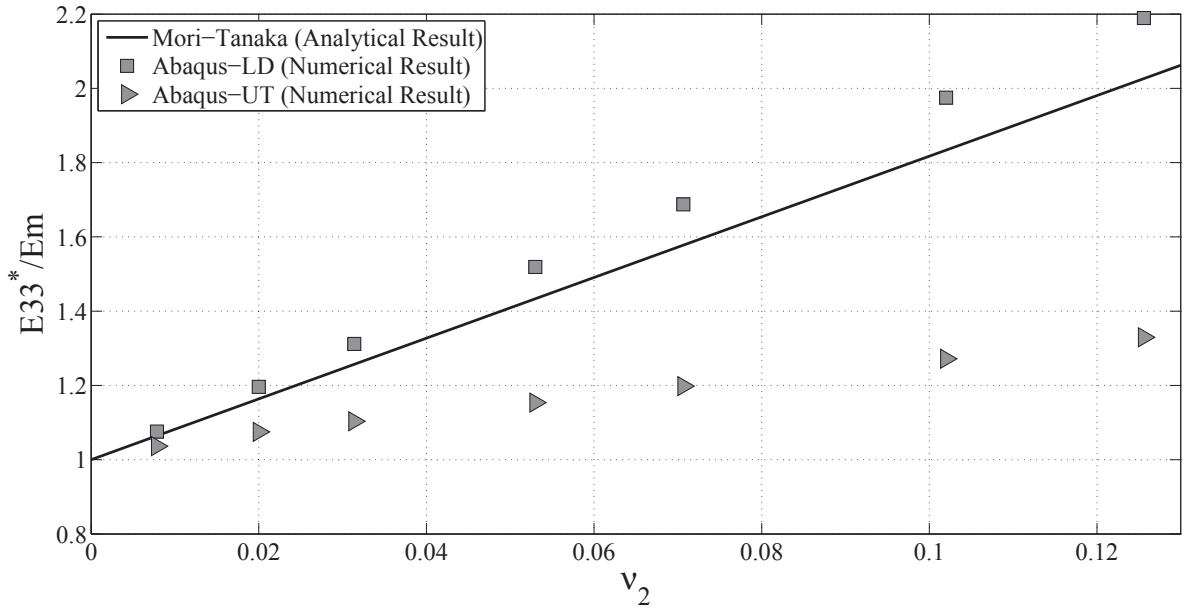

(a)

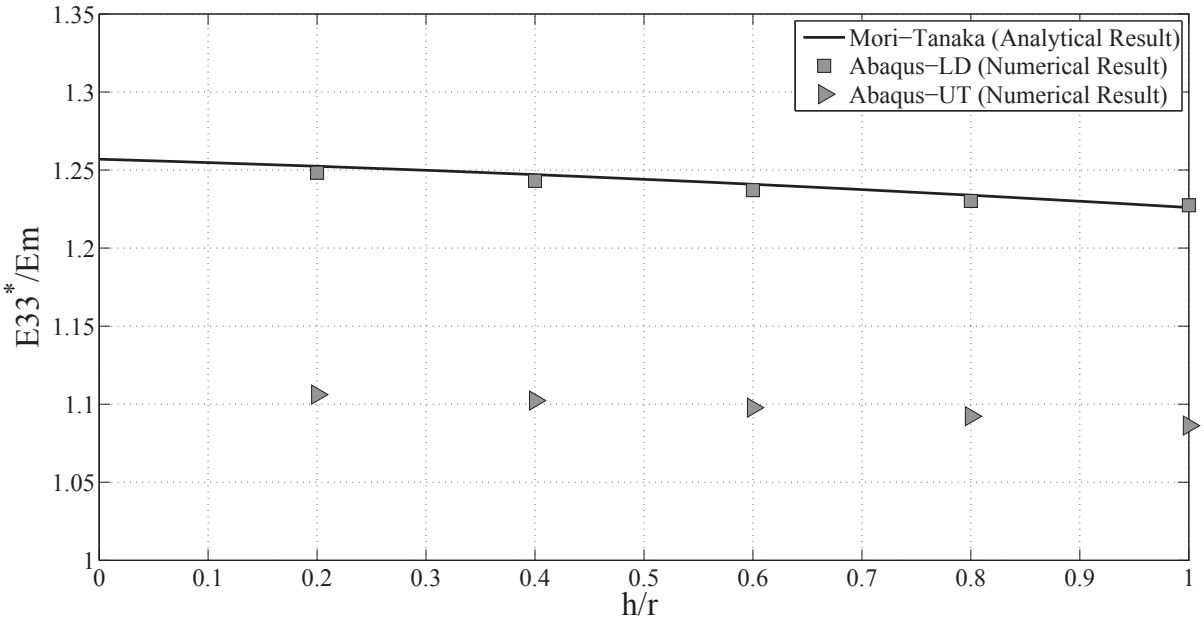

(b)

Figure 3.12: Normalized homogenized Young's modulus ($E33^*$/Em) of diamond reinforced copper matrix in transverse direction of cylinder vs: (a) volume fraction of cylinder inclusion (ν_2), (b) normalized interphase thickness (h/r), for the constant particle volume fraction of $\nu_2 = 0.0314$.

Chapter 4

Numerical investigation of interfacial effects

Beside the experimental methods, there are some analytical and numerical methods to calculate the overall effective elastic properties of nanocomposites. In this study, the finite element method was used to predict the elastic properties of nanocomposites in presence of the interphase layer. In essence this method is called the hierarchical multiscale method [42]. The hierarchical multiscale method has three main components: the approximation method (here we use finite elements), the upscaling method (computational homogenization) and the boundary conditions which are explained in the sequel.

4.1 Finite element model

We first create a finite element model of the representative volume element (RVE) from the system in hand which contains also the interfacial region along with the clays and the epoxy matrix. The clays are randomly distributed in the RVE. We used a quadrilateral plane stress (CPS4) elements with global approximate element size of 5nm to mesh the RVEs. Fig. 4.1 shows a detailed view of the mesh around the clays. The mesh has a single element through the thickness of interphase zone as well as clay thickness.

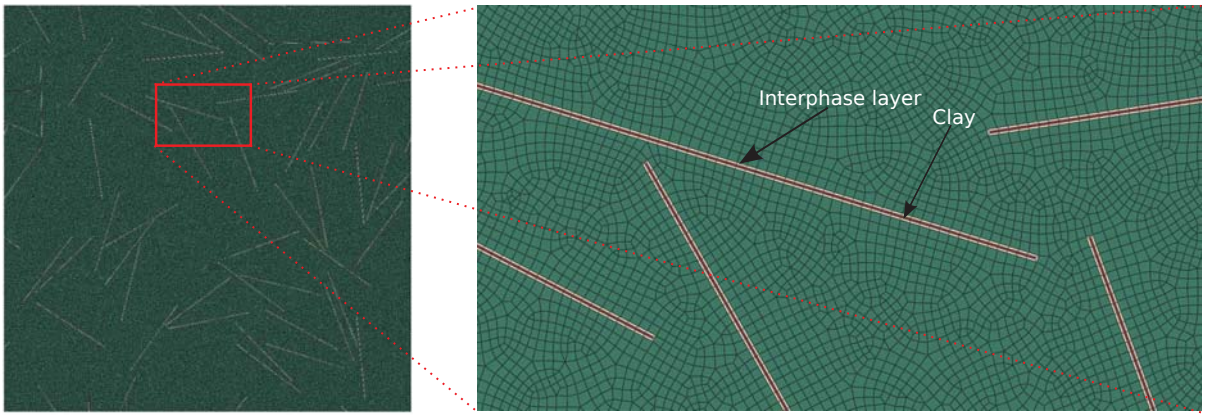

Figure 4.1: The finite element mesh of a sample RVE with a detailed view of the mesh near to the interphase layer

4.2 Boundary Conditions

There are three types of widely used boundary conditions (BCs) that are utilizable in homogenization procedures: linear displacement (LD) boundary condition, uniform traction (UT) boundary condition and periodic (PR) boundary condition [32]. LD and UT can provide upper and lower bounds for the elastic material constants respectively. In this study linear displacement boundary conditions was used to apply desirable amount of strain on the RVE. Please note that since the relative size of the clays to RVE dimensions and the volume ratio of the clays inside the RVE is small, the upper and lower bounds for Young's modulus of nanocomposites provided by LD and UT methods are very close to each other in the current study.

4.3 Stochastic Analysis

Fig.4.2 shows the flowchart of the stochastic analysis which is used in the current study. Three main boxes can be distinguished in the flowchart: design of experiments box, RVE generation box and homogenization box.

4.3.1 Design of Experiments (DoE)

There are different schemes to scan the space of the input variables. Regular arrangement of the samples (deterministic DoE) usually increases the number of the samples exponentially with increasing dimension. These approach are not efficient when the cost of each realization is high. As an alternative, stochastic DoE can be used. Mont Carlo Simulation (MCS) is a very comon option which is based on the random independent sampling in the given design space. MCS suffers from the existence of undesired correlations between the input variables which can affect the sensitivity measure significantly [43]. Latin Hypercube Sampling (LHS) [44] method was introduced as a remedy against this undesirable correlation. This method is recommended when the cost of each realization is high and we have less than 50 input parameters. LHS represents the input distributions very accurately even for small number of samples. LHS also minimize the unwanted correlation of the input variables. Advanced Latin Hypercube Sampling (ALHS) uses the stochastic evolution strategies [45] to minimize the correlation errors.

In this study, ALHS algorithm provided by Optislang software [46] was employed. We coupled Optislang with Abaqus [47] through Batch Jobs. Here the focus is only to study the effect of interphase layer on the Young's modulus of clay/epoxy nanocomposites and hence, we only considered the Young's modulus and thickness of the interphase layer as the stochastic inputs and set other parameters to be deterministic inputs with their mean value (the clay aspect ratio is considered to be 300 [28, 48] and the Young's modulus and Poisson's ratio of the epoxy and clays are considered as $1.96\,GPa$, $\nu = .25$, $221.5\,GPa$ and $\nu = .25$ [49, 28] respectively). To evaluate the effect of other inputs on the Young's modulus of clay/epoxy nanocomposites, refer to [24, 25]. Based on MD simulations and analytical results available in the literature the thickness and the Young's modulus of the interphase layer vary from $0.5\,nm$ to $2\,nm$ [17, 50] and $0.35\,Gpa$ to $1.96\,GPa$ [11], respectively.

4.3.2 RVE generation algorithm

The second dashed box in Fig.4.2 shows the RVE generation algorithm for PCNs with interphase layer. We used python scripting inside Abaqus/CAE to generate the RVEs. Having the values for the Young's modulus and thickness of interphase layer from Op-

tislang software as well as the other deterministic inputs, the RVE generation can be started.

Based on the RVE dimensions, volume ratio and clay dimensions, the number of clays inside the RVE can be determined. We used the random sequential addition algorithm (RSA) to position and orient the clays inside the RVE. The condition of non-overlapping and non-intersecting between clays was also satisfied. Since we have random generation algorithm for positioning and orienting the clays inside matrix, the RVEs do not show complete isotropic behaviour which is not consistent with the macroscopic isotropic behaviour of the PCNs. To overcome the undesirable anisotropic behaviour of the RVEs, a pairwise positioning algorithm was used to generate the clays in a sequential way. Fig.4.3 shows schematically this process. In each step, a pair of orthogonal clays was generated and positioned inside the RVE. This algorithm guarantees the isotropic behaviour of the RVEs.

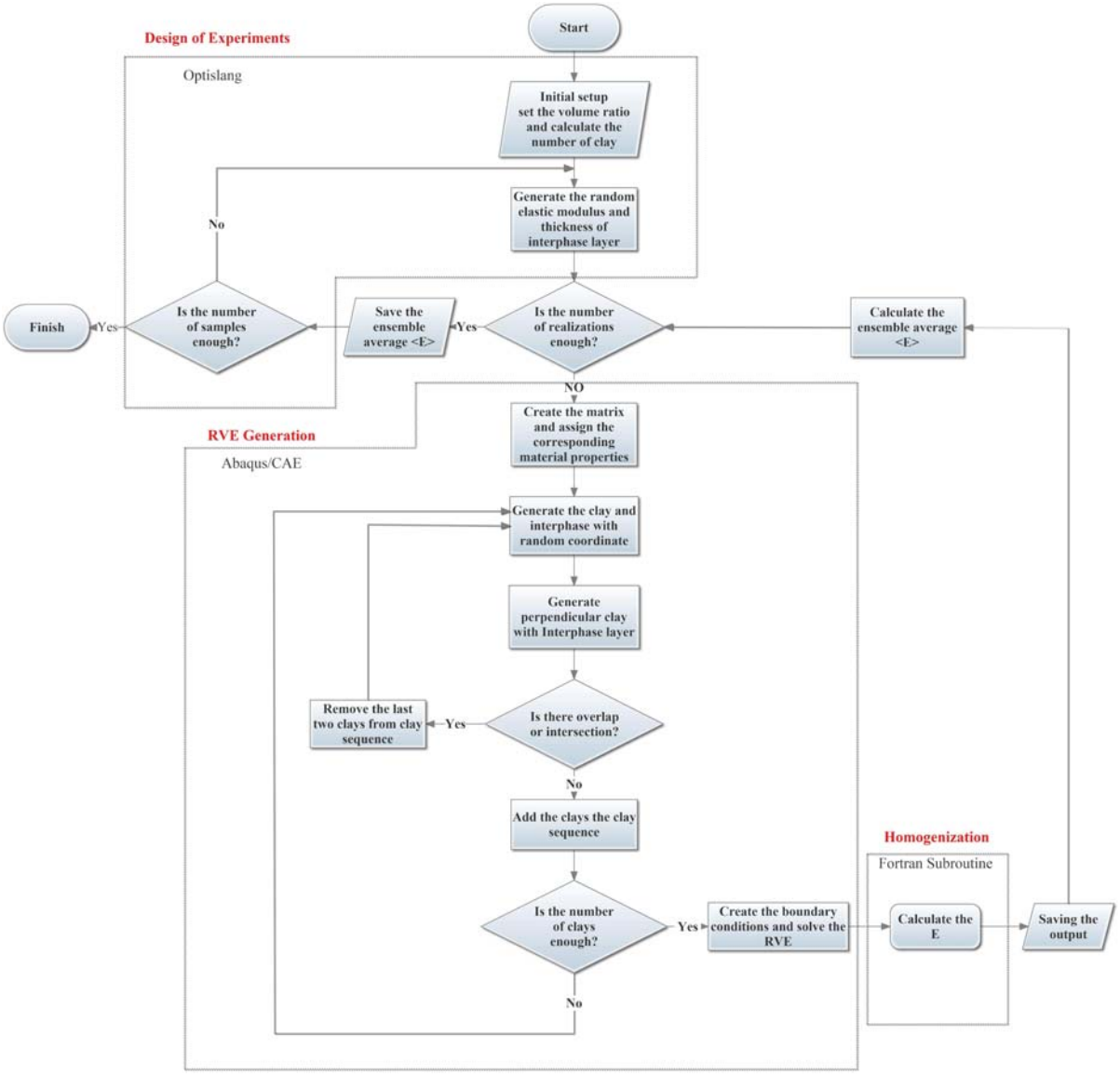

Figure 4.2: Flowchart of stochastic modeling processes.

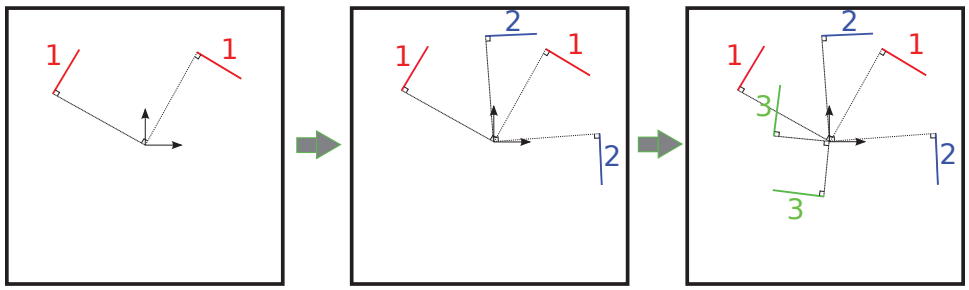

Figure 4.3: Schematic representation of pairwise positioning algorithm to generate isotropic RVEs.

4.4 Results and discussion

4.4.1 Ensemble averaging

To remove the effect of randomness of the positioning and orienting clays inside matrix on the outputs, the process of ensemble averaging should be performed. Accordingly, the following saturation criterion should be met:

$$| \frac{\langle\langle E \rangle\rangle^{(2J)} - \langle\langle E \rangle\rangle^{(J)}}{\langle\langle E \rangle\rangle^{(2J)}} | < Tol \tag{4.1}$$

where $\langle\langle\ \rangle\rangle^{(J)}$ implies an ensemble average using j realisations, and $\langle\langle\ \rangle\rangle^{(2J)}$ represent the same quantity obtained using twice this number of realisations. Tol is a convergence tolerance for ensemble averaging and determines the accuracy of the operation. To simplify the numerical procedure, a 2 wt% clay/epoxy nanocomposite was considered and an ensemble averaging test was conducted. The dimension of the RVE is considered as $1500 \times 1500\, nm^2$ [25]. Fig. 4.4 shows the average Young's modulus for 2 wt% clay/epoxy nanocomposite versus the realization number. The figure clearly shows that the convergence would be guaranteed for 50 realizations with a convergence error of less than 0.03 %.

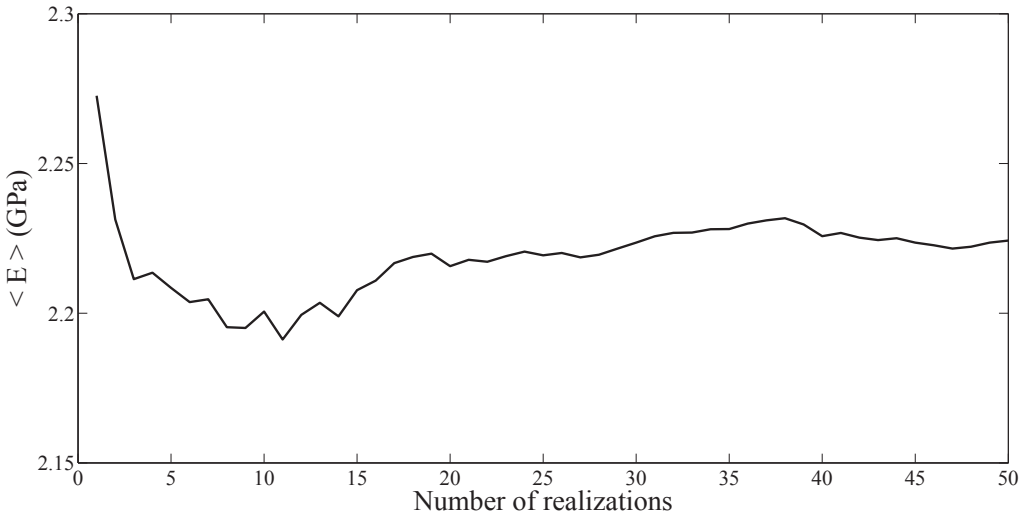

Figure 4.4: The average Young's modulus for 2 wt% clay/epoxy nanocomposite versus realization number.

4.4.2 Young's modulus of clay/epoxy nanocomposites

Table.4.1 summarises the results of the stochastic analysis. The table shows the mean values and standard deviation of the Young's modulus for 0.5 wt%, 1 wt%, 2 wt% and 3 wt% clay/epoxy nanocomposites. As it is expected, the Young's modulus of the clay/epoxy nanocomposites increases with increasing in the clay contents.

Table 4.1: The mean value and standard deviation (SD) of the Young's modulus for different weight percentage of the clay

Clay percentage (wt%)	Mean value of E (GPa)	Standard deviation of E (GPa)
0.5%	2.042	0.0443
1%	2.1065	0.0435
2%	2.2303	0.0507
3%	2.3375	0.0836

To validate the results of stochastic analysis with experimental results, Fig.4.5 plots the results of Table.4.1 as well as experimental results of Wang et al.[28]. The predicted numerical results are in good agreement with the experimental values with the maximum error less than 6%. This figure also includes the numerical results of Silani et al. [25] for the same problem but neglecting the interphase layer. The figure represents that the Young's modulus of clay/epoxy nanocomposite rises gradually with increasing in the clay percentage both in the experimental and in the numerical results. It also shows considering interphase layer in the numerical simulations reduces the Young's modulus of clay/epoxy nanocomposite and this decrease becomes significant in higher clay contents which means that the effect of intephase layer is considerable in high clay weight ratios.

Fig. 4.6 shows the histograms of the Young's modulus of clay/epoxy nanocomposites based on the current stochastic analysis. To find and fit an appropriate probability distribution function to these results, the chi-square goodness-of-fit test [51] was performed for lognormal, weibull and logistic distribution. The results demonstrate that the Chi-square test accepts the logistic distribution function at 4% significance level and hence, we used logistic distribution fit in Fig. 4.6. The respective logistic probability plot for different clay concentration are drawn in the Fig.4.7.

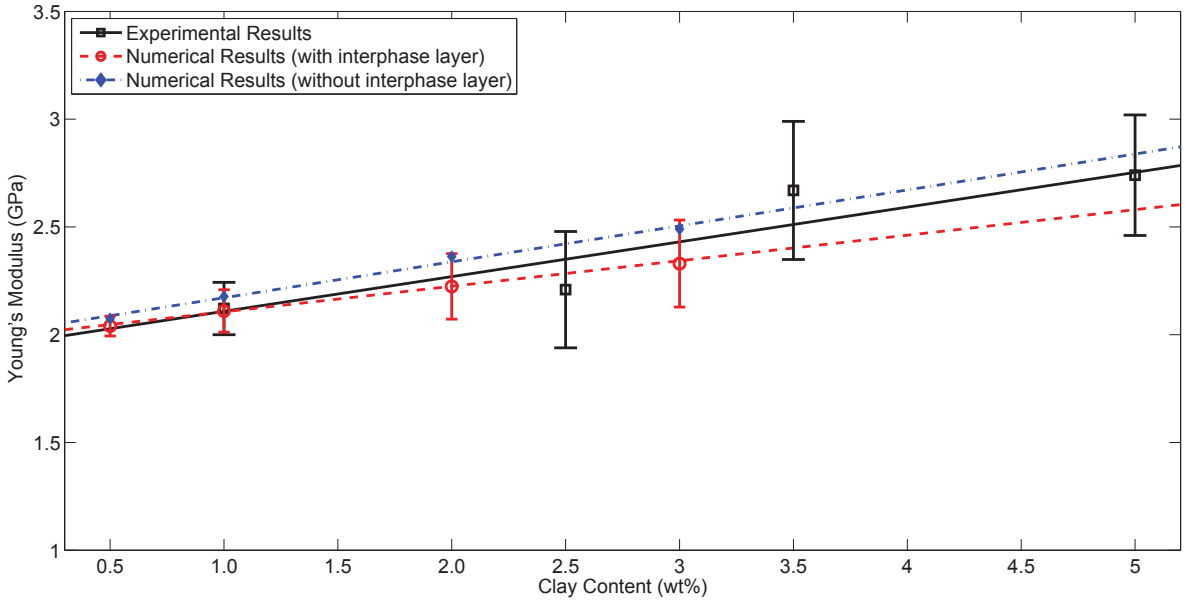

Figure 4.5: Experimental and numerical Young's modulus of clay/epoxy nanocomposite with considering the effect of interphase layer versus clay concentration. Experimental results are from [28] and numerical results without interphase layer are from [25].

4.4.3 Polynomial based sensitivity analysis

Polynomial regression is a common approximation method in which the model response is generally approximated by a polynomial basis function of linear or quadratic order with or without coupling terms. The estimated regression line is defined as [52]:

$$\hat{y} = \hat{\beta}_0 + \hat{\beta}_1 x, \tag{4.2}$$

with $\hat{\beta}_0$ and $\hat{\beta}_1$ defined as:

$$\hat{\beta}_0 = \bar{y} - \hat{\beta}_1 \bar{x}, \qquad \hat{\beta}_1 = \frac{S_{xy}}{S_{xx}}, \qquad S_{xx} = \sum_{i=1}^{n} x_i^2 - n\bar{x}^2, \qquad S_{xy} = \sum_{i=1}^{n} y_i x_i - n\bar{x}\bar{y}. \tag{4.3}$$

In Eq. 4.3, x_i and y_i are inputs and outputs, $\bar{x}$ and $\bar{y}$ are mean values of the inputs and outputs and n is the number of observations. Coefficients $\hat{\beta}_0$ and $\hat{\beta}_1$ are the intercept and the slope of regression line respectively.

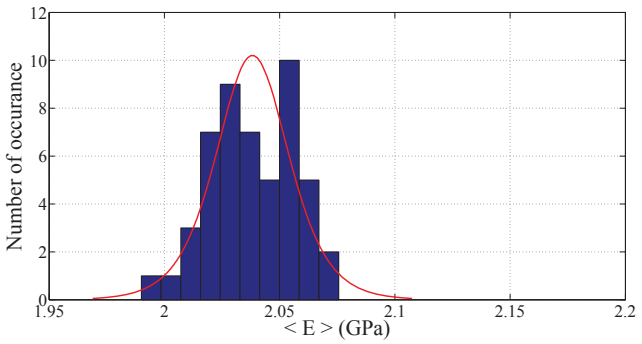

(a)

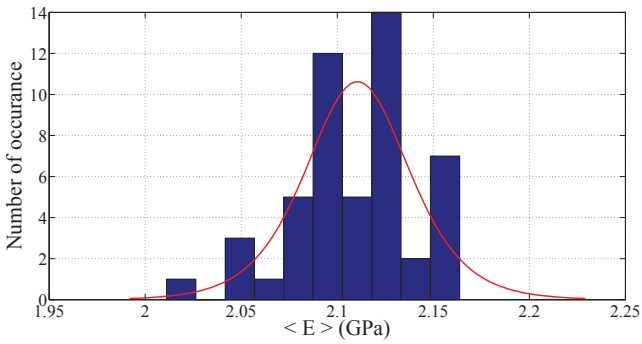

(b)

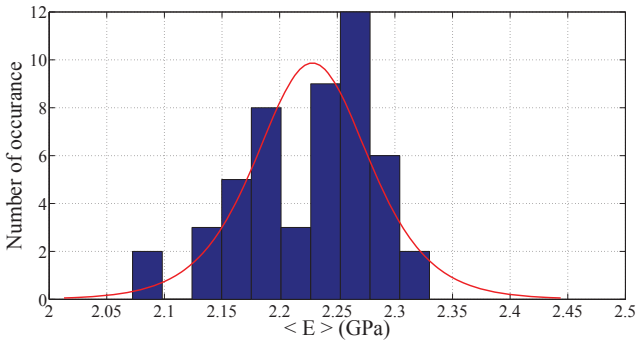

(c)

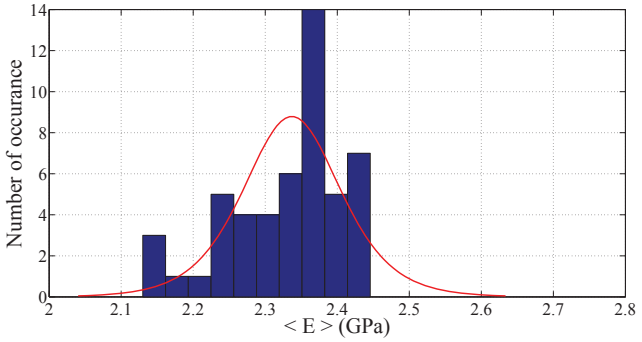

(d)

Figure 4.6: Histogram of Young's modulus for (a) 0.5 wt% (b) 1 wt% (c) 2 wt% (d) 3 wt% clay/epoxy nanocomposite. The solid line corresponds to Logistic distribution fit.

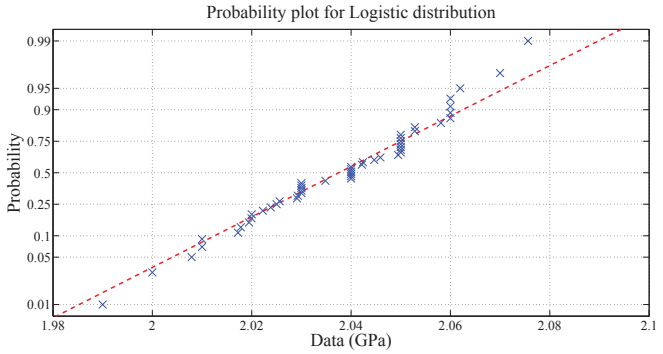

(a)

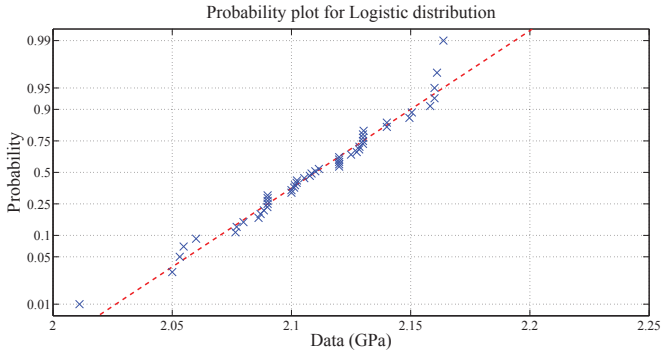

(b)

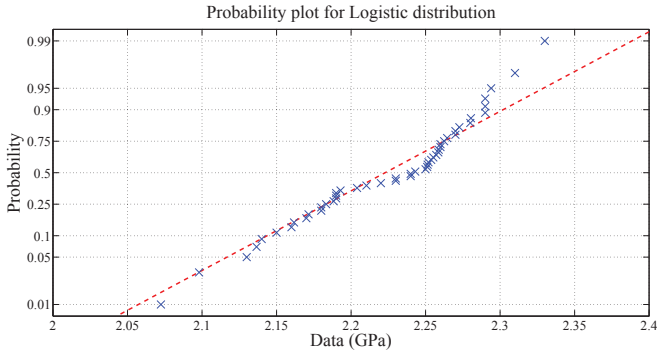

(c)

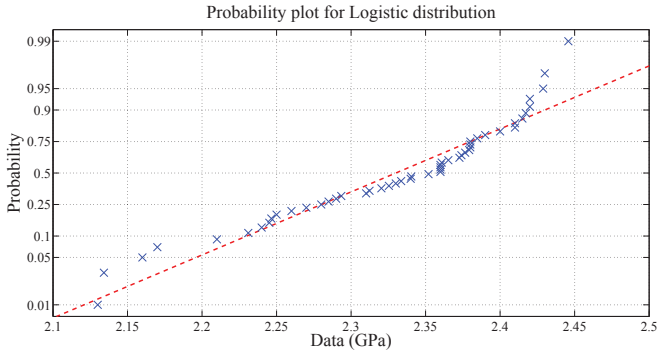

(d)

Figure 4.7: Logistic probability plot for the distribution of Young's modulus E for (a) 0.5 wt% (b) 1 wt% (c) 2 wt% (d) 3 wt% clay/epoxy nanocomposite.

In order to quantify the effect of interphase layer on the Young's modulus of clay/epoxy nanocomposites, the sensitivity analysis was performed. The linear regression model was used to compute the intercept ($\hat{\beta}_0$) and slope ($\hat{\beta}_1$) of regression line for different clay weight ratios. The intercept and slope of the linear regression model for Young's modulus of clay/epoxy nanocomposites are listed in Table 4.2 and 4.3 respect to the thickness and Young's modulus of interphase layer respectively. The results clearly shows that the Young's modulus of interphase layer has more significant effect on the stiffness of clay/epoxy nanocomposites.

Table 4.2: The intercept and the slope of linear regression model for Young's modulus of clay/epoxy nanocomposites versus thickness of interphase.

	0.5% clay	1%clay	2%clay	3%clay
Intercept ($\hat{\beta}_0$)	2.0572	2.1225	2.2744	2.4035
Slope ($\hat{\beta}_1$)	−0.0157	−0.0105	−0.0400	−0.0596

Table 4.3: The intercept and the slope of linear regression model for Young's modulus of clay/epoxy nanocomposites versus Young's modulus of interphase.

	0.5% clay	1%clay	2%clay	3%clay
Intercept ($\hat{\beta}_0$)	2.0155	2.0538	2.1402	2.1824
Slope ($\hat{\beta}_1$)	0.0191	0.0481	0.0728	0.1268

In order to estimate the approximation quality of a polynomial regression model, the Coefficient of Determination (CoD) can be used. This measure is defined as the relative amount of variation explained by the approximation [52]

$$R^2 = \frac{SS_R}{SS_T} = 1 - \frac{SS_E}{SS_T}, \quad 0 \leq R^2 \leq 1, \tag{4.4}$$

where SS_E is the error sum of squares

$$SS_E = \sum_{i=1}^{n} e_i^2 = \sum_{i=1}^{n} (y_i - \hat{y}_i)^2 = SS_T - \hat{\beta}_1 S_{xy}, \tag{4.5}$$

SS_T is the total sum of squares

$$SS_T = \sum_{i=1}^{n}(y_i - \bar{y})^2 = \sum_{i=1}^{n}(\hat{y}_i - \bar{y})^2 + \sum_{i=1}^{n}(y_i - \hat{y}_i)^2, \tag{4.6}$$

and SS_R is the regression sum of squares

$$SS_R = \sum_{i=1}^{n}(\hat{y}_i - \bar{y})^2. \tag{4.7}$$

Accordingly, the variance of error term ϵ ($n-2$ degrees of freedom) can be expressed as

$$\hat{\sigma}^2 = \frac{SS_E}{n-2}. \tag{4.8}$$

Table 4.4 and 4.5 show the values of CoD (R^2) and the variance error ($\hat{\sigma}^2$) of the regression line for different clay weight ratio respect to thickness and modulus of interphase layer respectively.

Table 4.4: CoD result summary with respect to thickness of interphase.

	0.5% clay	1%clay	2%clay	3%clay
SS_T	0.0164	0.0508	0.1578	0.3133
SS_R	0.0023	0.0011	0.0151	0.0336
SS_E	0.0141	0.0498	0.1427	0.2797
R^2	0.1412	0.0207	0.0956	0.1071
$\hat{\sigma}^2$	0.0003	0.0010	0.0030	0.0058

Table 4.5: CoD result summary with respect to modulus of interphase.

	0.5% clay	1%clay	2%clay	3%clay
SS_T	0.0164	0.0508	0.1578	0.3133
SS_R	0.0040	0.0249	0.0572	0.1735
SS_E	0.0125	0.0259	0.1006	0.1398
R^2	0.2408	0.4902	0.3626	0.5539
$\hat{\sigma}^2$	0.0003	0.0005	0.0021	0.0029

The confidence interval of mean response at $x = x_0$ can also be written as

$$\hat{\mu}_{Y|x_0} - t_{\alpha/2,n-2}\sqrt{\hat{\sigma}^2\left[\frac{1}{n} + \frac{(x_0 - \bar{x})^2}{S_{xx}}\right]} \leq \mu_{Y|x_0} \leq \hat{\mu}_{Y|x_0} + t_{\alpha/2,n-2}\sqrt{\hat{\sigma}^2\left[\frac{1}{n} + \frac{(x_0 - \bar{x})^2}{S_{xx}}\right]} \tag{4.9}$$

where $t_{p,\nu}$ is the inverse of Student's t cdf using the degrees of freedom in ν for the corresponding probabilities in p [52].

Figs. 4.8, 4.9, 4.10, 4.11 show the scater plot of Young's modulus of clay/epoxy nanocomposite versus the interphase thickness and the Young's modulus of interphase region for different clay weight ratios. The regions with 95% Confidence intervals (CIs) and 95% Prediction intervals (PIs) are also depicted in these figures. The 95% CIs corresponds to the area which lies between the red lines while the region between the green lines corresponds to the 95% PIs. CIs demonstrate how well we have determined the mean and tell the likely location of the true population parameter while PIs tell about the distribution of values and where we can expect the next data point. Since that prediction interval accounts for both the uncertainty in knowing the value of the population mean plus data scatter, the PIs is always wider than CIs.

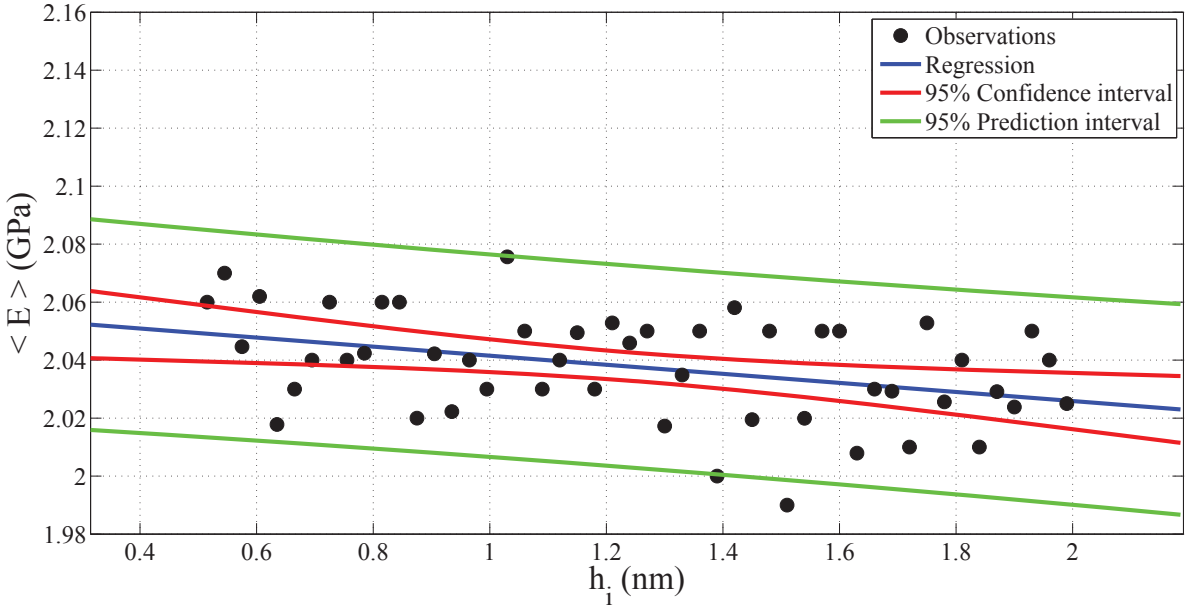

(a)

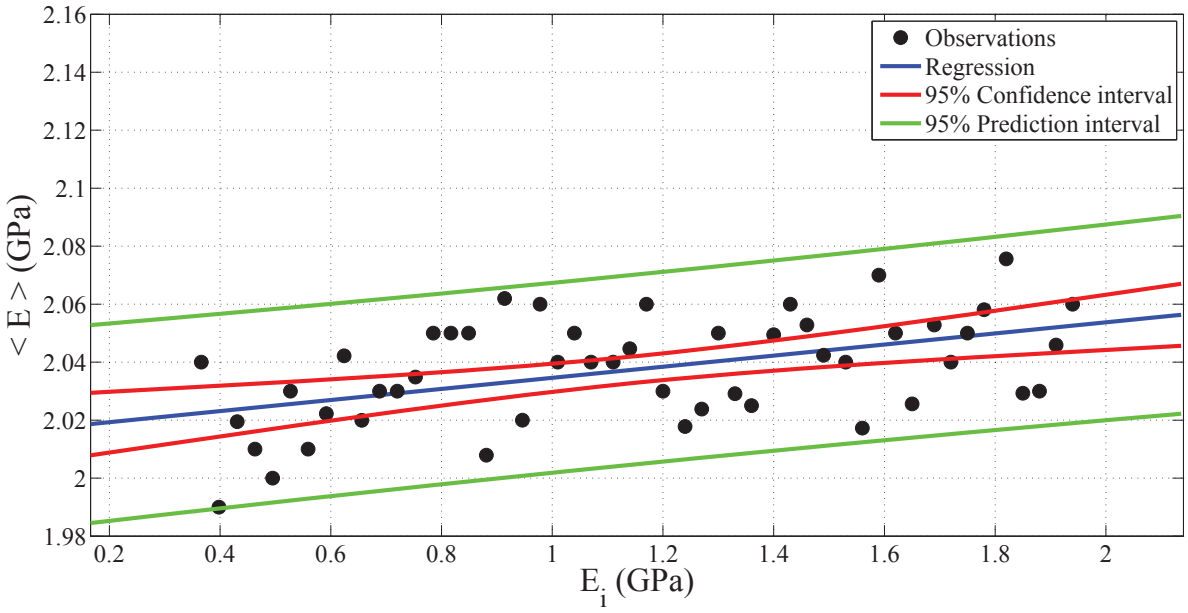

(b)

Figure 4.8: Young's modulus of 0.5 wt% clay/epoxy nanocomposites versus (a) interphse thickness and (b) Young's modulus of interphase region.

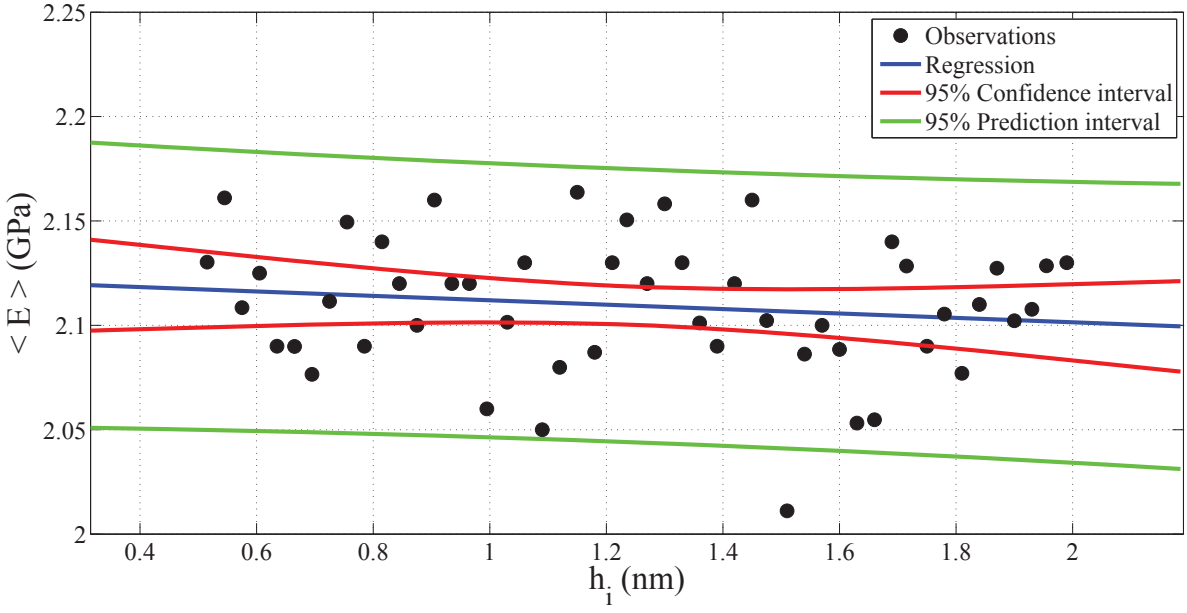

(a)

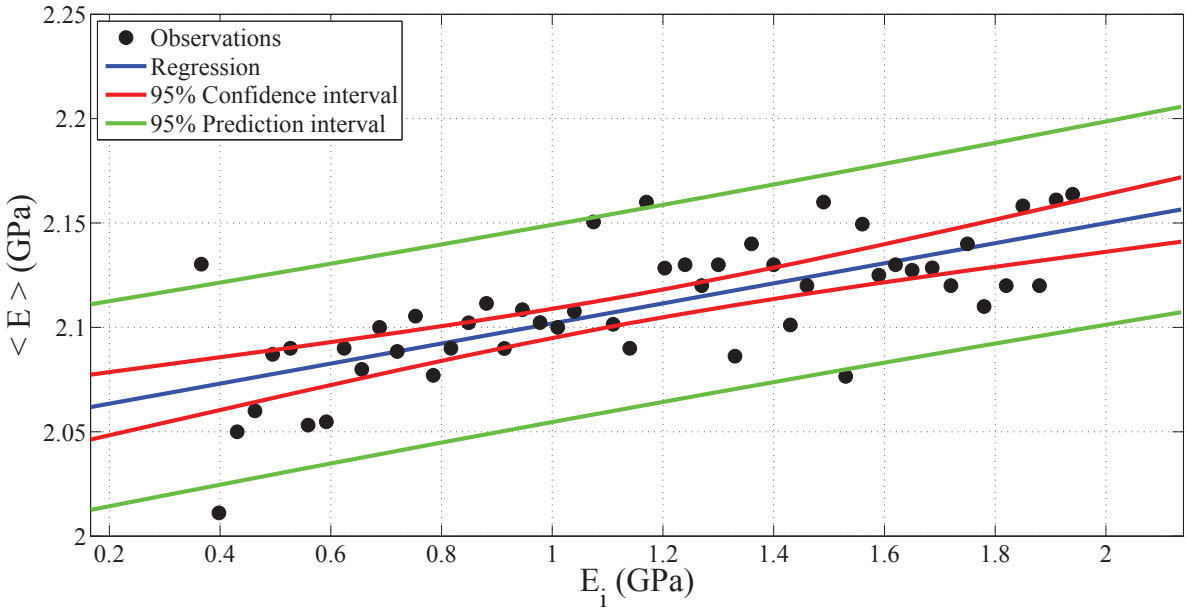

(b)

Figure 4.9: Young's modulus of 1 wt% clay/epoxy nanocomposites versus (a) interphse thickness and (b) Young's modulus of interphase region.

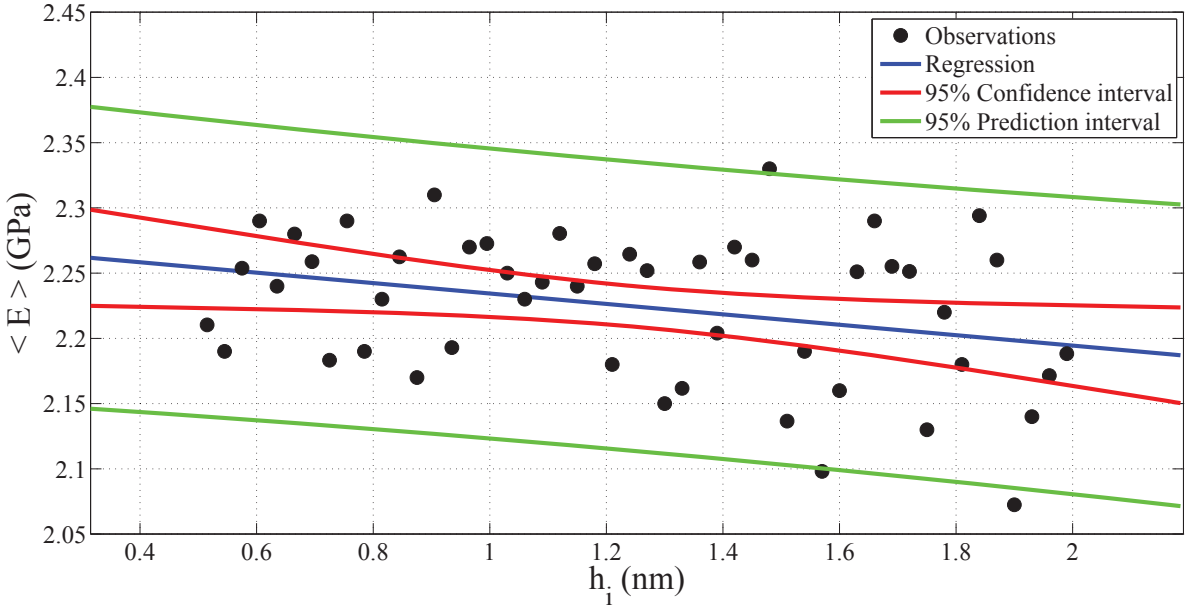

(a)

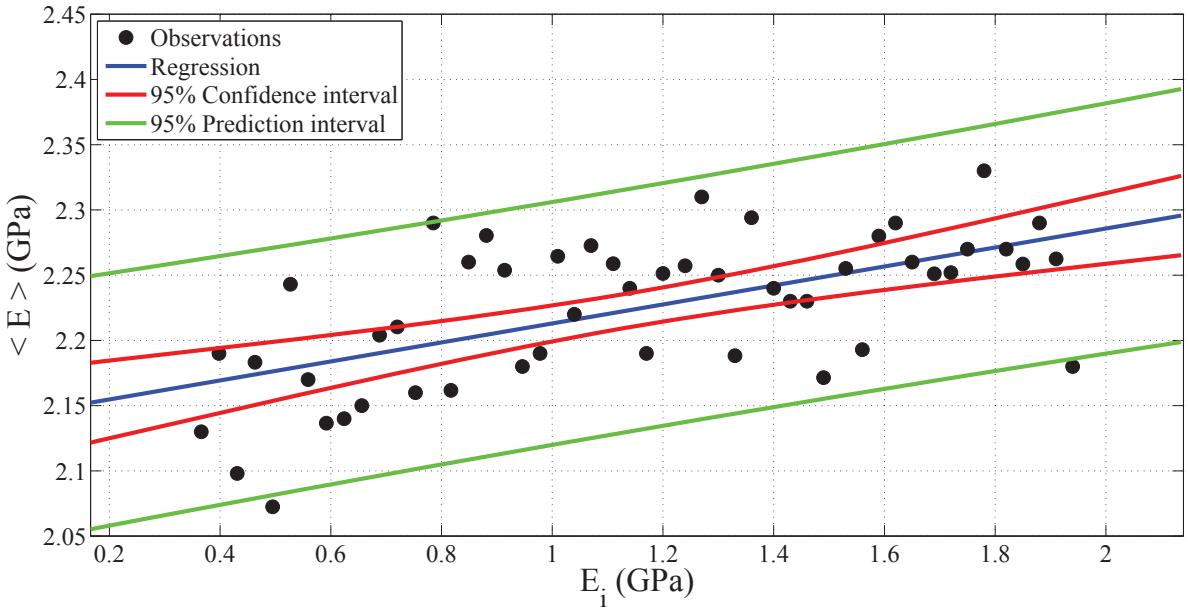

(b)

Figure 4.10: Young's modulus of 2 wt% clay/epoxy nanocomposites versus (a) interphse thickness and (b) Young's modulus of interphase region.

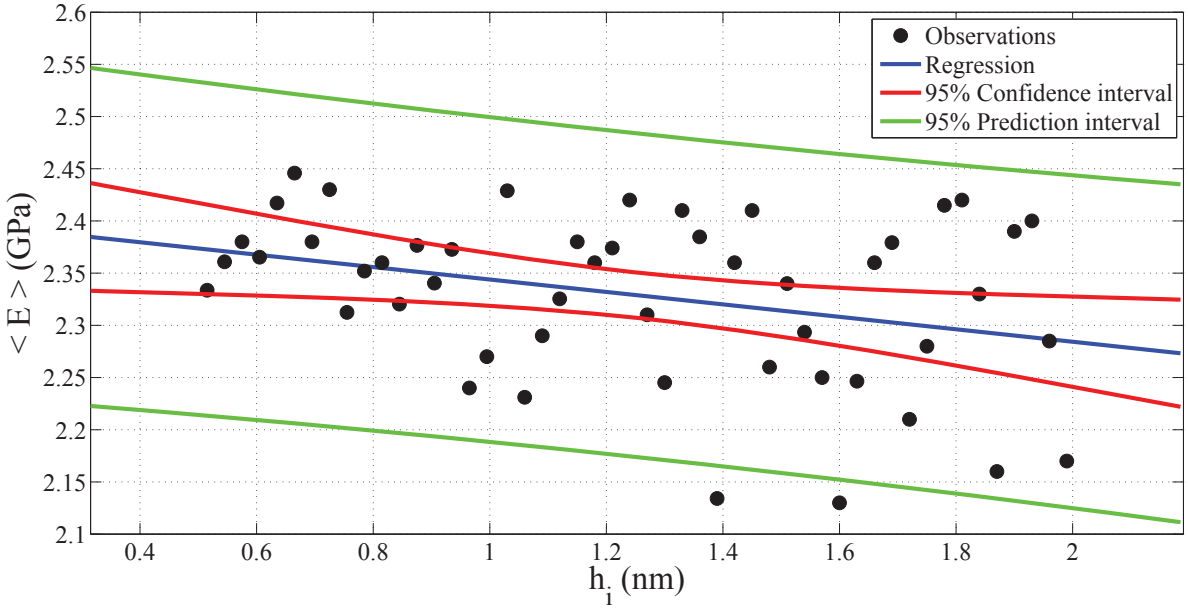

(a)

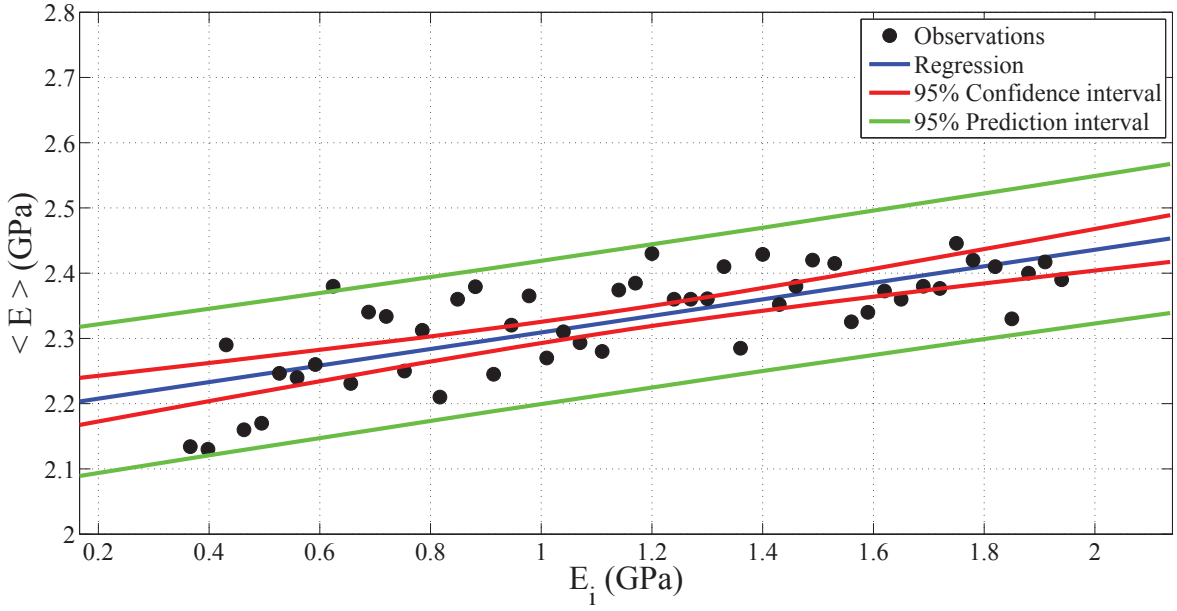

(b)

Figure 4.11: Young's modulus of 3 wt% clay/epoxy nanocomposites versus (a) interphse thickness and (b) Young's modulus of interphase region.

Chapter 5

Conclusions and future works

5.1 Conclusions

In this thesis, different analytical methods are first introduced, and Mori-Tanaka method is then utilized to investigate the overall elastic properties of simple inclusion geometries of cylinder and sphere. Furthermore, the effect of interphase region on the overall properties of composites is studied. We obtain a precise bound for the effective mechanical properties of the composites using FEM analysis. For this, the linear displacement boundary conditions (LD) and uniform traction boundary conditions (UT) are simulated using FEM models. The numerical results are in excellent agreement with those obtained from analytical results.

In this study we used the computational homogenization along with the stochastic analysis to study the effect of the interphase between the clays and the epoxy matrix on the overall mechanical properties of the clay/epoxy nanocomposite. The finite element models of the representative volume elements (RVEs) were generated according to a procedure which guaranties the randomness and also the isotropic behaviour of the RVEs. A total number of 200 RVEs were simulated for a stochastic analysis and the resultant Young's modulus were computed using computational homogenisation.

To approximate the Young's modulus, we used the polynomial regression model and investigated the approximation quality with the Coefficient of Determination (CoD) measure. The results of this study prove that the interphase layer becomes significant

only in high clay weight ratios. The sensitivity analysis also show that the stiffness of interphase layer has more significant effect on the final stiffness of nanocomposites compare to thickness of interphase layer. The results of this study were validated with available experimental results with the maximum error less than 6%.

5.2 Future Works

In this work, we used 2D RVEs to investigate the effects of interphase layer on the mechanical properties of clay/epoxy nanocomposites. Using the 3D models give a more realistic results especially for disc shape clays. Here, we coupled FEM with stochastic analysis to predict the Young's modulus clay/epoxy nanocomposites. Coupling analytical methods such as Mori-Tanaka with the stochastic scheme can also give valuable information about the effects of inputs. Finally, the extension current study to model the fracture and damage in nanocomposites is proposed.

REFERENCES

[1] RE Grim. Clay minerals. *Clay minerals*, 1968.

[2] M.W. Ho, C.K. Lam, K. Lau, D.H.L. Ng, and D. Hui. Mechanical properties of epoxy-based composites using nanoclays. *Composite structures*, 75(1):415–421, 2006.

[3] Jeffrey Jordan, Karl I Jacob, Rina Tannenbaum, Mohammed A Sharaf, and Iwona Jasiuk. Experimental trends in polymer nanocompositesa review. *Materials science and engineering: A*, 393(1):1–11, 2005.

[4] Linda S Schadler, Sanat K Kumar, Brian C Benicewicz, Sarah L Lewis, and Shane E Harton. Designed interfaces in polymer nanocomposites: A fundamental viewpoint. *MRS bulletin*, 32(04):335–340, 2007.

[5] Tatsuki Ohji, Takeshi Hirano, Atsushi Nakahira, and Koichi Niihara. Particle/matrix interface and its role in creep inhibition in alumina/silicon carbide nanocomposites. *Journal of the American Ceramic Society*, 79(1):33–45, 1996.

[6] Béla Pukánszky. Interfaces and interphases in multicomponent materials: past, present, future. *European Polymer Journal*, 41(4):645–662, 2005.

[7] M Roy, JK Nelson, RK MacCrone, LS Schadler, CW Reed, and R Keefe. Polymer nanocomposite dielectrics-the role of the interface. *Dielectrics and Electrical Insulation, IEEE Transactions on*, 12(4):629–643, 2005.

[8] GM Odegard, TC Clancy, and TS Gates. Modeling of the mechanical properties of nanoparticle/polymer composites. *Polymer*, 46(2):553–562, 2005.

[9] T Mori and K Tanaka. Average stress in matrix and average elastic energy of materials with misfitting inclusions. *Acta metallurgica*, 21(5):571–574, 1973.

[10] Y1 Benveniste. A new approach to the application of mori-tanaka's theory in composite materials. *Mechanics of materials*, 6(2):147–157, 1987.

[11] Igor Sevostianov and Mark Kachanov. Effect of interphase layers on the overall elastic and conductive properties of matrix composites. applications to nanosize inclusion. *International Journal of Solids and Structures*, 44(3):1304–1315, 2007.

[12] Genzo Tanaka and Lloyd A Goettler. Predicting the binding energy for nylon 6, 6/clay nanocomposites by molecular modeling. *Polymer*, 43(2):541–553, 2002.

[13] Radovan Toth, Alessandro Coslanich, Marco Ferrone, Maurizio Fermeglia, Sabrina Pricl, Stanislav Miertus, and Emo Chiellini. Computer simulation of polypropylene/organoclay nanocomposites: characterization of atomic scale structure and prediction of binding energy. *Polymer*, 45(23):8075–8083, 2004.

[14] Giulio Scocchi, Paola Posocco, Jan-Willem Handgraaf, JohannesG.E.M. Fraaije, Maurizio Fermeglia, and Sabrina Pricl. A complete multiscale modelling approach for polymerclay nanocomposites. *Chemistry A European Journal*, 15(31):7586–7592, 2009.

[15] Qilu Zhang, Xiaoyan Ma, Yifei Wang, and Kaichang Kou. Morphology and interfacial action of nanocomposites formed from ethylene- vinyl acetate copolymers and organoclays. *The Journal of Physical Chemistry B*, 113(35):11898–11905, 2009.

[16] Y Chen, JYH Chia, ZC Su, TE Tay, and VBC Tan. Mechanical characterization of interfaces in epoxy-clay nanocomposites by molecular simulations. *Polymer*, 54(2):766–773, 2013.

[17] Jia-Lin Tsai, Shi-Hua Tzeng, and Yu-Tsung Chiu. Characterizing elastic properties of carbon nanotubes/polyimide nanocomposites using multi-scale simulation. *Composites Part B: Engineering*, 41(1):106–115, 2010.

[18] B Arash, Q Wang, and VK Varadan. Mechanical properties of carbon nanotube/polymer composites. *Scientific reports*, 4, 2014.

[19] M.R. Ayatollahi, S. Shadlou, and M.M. Shokrieh. Multiscale modeling for mechanical properties of carbon nanotube reinforced nanocomposites subjected to different types of loading. *Composite Structures*, 93(9):2250 – 2259, 2011.

[20] P.D. Spanos and A. Kontsos. A multiscale monte carlo finite element method for determining mechanical properties of polymer nanocomposites. *Probabilistic Engineering Mechanics*, 23(4):456 – 470, 2008.

[21] K.I. Tserpes, P. Papanikos, G. Labeas, and Sp.G. Pantelakis. Multi-scale modeling of tensile behavior of carbon nanotube-reinforced composites. *Theoretical and Applied Fracture Mechanics*, 49(1):51 – 60, 2008.

[22] K.I. Tserpes, G. Labeas, and S. Pantelakis. Multi-scale modeling of the mechanical response of plain weave composites and cellular solids. *Theoretical and Applied Fracture Mechanics*, 54(3):172 – 179, 2010.

[23] Mahmood M. Shokrieh and Roham Rafiee. Stochastic multi-scale modeling of cnt/polymer composites. *Computational Materials Science*, 50(2):437 – 446, 2010.

[24] N Vu-Bac, M Silani, T Lahmer, X Zhuang, and T Rabczuk. A unified framework for stochastic predictions of mechanical properties of polymeric nanocomposites. *Computational Materials Science*, 2014.

[25] Mohammad Silani, Hossein Talebi, Saeed Ziaei-Rad, Pierre Kerfriden, Stéphane PA Bordas, and Timon Rabczuk. Stochastic modelling of clay/epoxy nanocomposites. *Composite Structures*, 118:241–249, 2014.

[26] MC Boyce, DM Parks, N Sheng, et al. Multiscale micromechanical modeling of the thermal/mechanical properties of polymer/clay nanocomposites [ph. d. thesis]. *Massachusetts Institute of Technology*, 2006.

[27] ALYSSA Downing-Perrault. Polymer nanocomposites are the future. *University of Wisconsin-Stout, Menomonie, Wis, USA*, 2005.

[28] Ke Wang, Ling Chen, Jingshen Wu, Mei Ling Toh, Chaobin He, and Albert F Yee. Epoxy nanocomposites with highly exfoliated clay: mechanical properties and fracture mechanisms. *Macromolecules*, 38(3):788–800, 2005.

[29] Clément Sanchez, Philippe Belleville, Michael Popall, and Lionel Nicole. Applications of advanced hybrid organic–inorganic nanomaterials: from laboratory to market. *Chemical Society Reviews*, 40(2):696–753, 2011.

[30] Suprakas Sinha Ray and Masami Okamoto. Polymer/layered silicate nanocomposites: a review from preparation to processing. *Progress in polymer science*, 28(11):1539–1641, 2003.

[31] Pham Hoai Nam, Pralay Maiti, Masami Okamoto, Tadao Kotaka, Takashi Nakayama, Mitsuko Takada, Masahiro Ohshima, Arimitsu Usuki, Naoki Hasegawa, and Hirotaka Okamoto. Foam processing and cellular structure of polypropylene/clay nanocomposites. *Polymer Engineering & Science*, 42(9):1907–1918, 2002.

[32] Ilker Temizer. *Lecture notes Micromechanics Analysis of Heterogeneous Materials*. Department of Mechanical Engineering Bilkent University, 2007.

[33] Tarek I Zohdi and Peter Wriggers. *An introduction to computational micromechanics*, volume 20. Springer, 2008.

[34] JOHN D Eshelby. The determination of the elastic field of an ellipsoidal inclusion, and related problems. *Proceedings of the Royal Society of London. Series A. Mathematical and Physical Sciences*, 241(1226):376–396, 1957.

[35] Z Hashin and S Shtrikman. On some variational principles in anisotropic and nonhomogeneous elasticity. *Journal of the Mechanics and Physics of Solids*, 10(4):335–342, 1962.

[36] Zvi Hashin and S Shtrikman. A variational approach to the theory of the elastic behaviour of multiphase materials. *Journal of the Mechanics and Physics of Solids*, 11(2):127–140, 1963.

[37] A Reuss. Berechnung der fließgrenze von mischkristallen auf grund der plastizitätsbedingung für einkristalle. *ZAMM-Journal of Applied Mathematics and Mechanics/Zeitschrift für Angewandte Mathematik und Mechanik*, 9(1):49–58, 1929.

[38] Woldemar Voigt. Ueber die beziehung zwischen den beiden elasticitätsconstanten isotroper körper. *Annalen der Physik*, 274(12):573–587, 1889.

[39] Toshio Mura. *Micromechanics of defects in solids*, volume 3. Springer, 1987.

[40] CR Weinberger, W Cai, and DM Barnett. Elasticity of microscopic structures. *ME340B Lecture Notes*, 2005.

[41] ML Dunn and H Ledbetter. Elastic moduli of composites reinforced by multiphase particles. *Journal of applied mechanics*, 62(4):1023–1028, 1995.

[42] Hossein Talebi, Mohammad Silani, Stéphane PA Bordas, Pierre Kerfriden, and Timon Rabczuk. A computational library for multiscale modeling of material failure. *Computational Mechanics*, 53(5):1047–1071, 2014.

[43] Reuven Y Rubinstein and Dirk P Kroese. *Simulation and the Monte Carlo method*, volume 707. John Wiley & Sons, 2011.

[44] Michael D McKay, Richard J Beckman, and William J Conover. Comparison of three methods for selecting values of input variables in the analysis of output from a computer code. *Technometrics*, 21(2):239–245, 1979.

[45] DE Huntington and CS Lyrintzis. Improvements to and limitations of latin hypercube sampling. *Probabilistic Engineering Mechanics*, 13(4):245–253, 1998.

[46] DYNARDO GmbH. Weimar. *optiSLang/sensitivity analysis, multidisciplinary optimization, robustness evaluation and reliability analysis, Version 4.1*, 2014.

[47] Hibbit, Karlsson and Sorensen Inc. *ABAQUS/Explicit User's Manual Version 6.12.1*, 2014.

[48] Ke Wang, Lei Wang, Jingshen Wu, Ling Chen, and Chaobin He. Preparation of highly exfoliated epoxy/clay nanocomposites by slurry compounding: process and mechanisms. *Langmuir*, 21(8):3613–3618, 2005.

[49] Biqiong Chen and Julian RG Evans. Elastic moduli of clay platelets. *Scripta materialia*, 54(9):1581–1585, 2006.

[50] Seunghwa Yang, Suyoung Yu, Junghyun Ryu, Jeong-Min Cho, Woomin Kyoung, Do-Suck Han, and Maenghyo Cho. Nonlinear multiscale modeling approach to characterize elastoplastic behavior of cnt/polymer nanocomposites considering the interphase and interfacial imperfection. *International Journal of Plasticity*, 41:124–146, 2013.

[51] Myles Hollander and Edsel A Peña. A chi-squared goodness-of-fit test for randomly censored data. *Journal of the American Statistical Association*, 87(418):458–463, 1992.

[52] Andrea Saltelli, Marco Ratto, Terry Andres, Francesca Campolongo, Jessica Cariboni, Debora Gatelli, Michaela Saisana, and Stefano Tarantola. *Global sensitivity analysis: the primer*. John Wiley & Sons, 2008.